Molecular Reaction Dynamics
Lectures 1-4

Claire Vallance

INTRODUCTION

By now you should be well and truly used to the concepts involved in reaction kinetics on a macroscopic scale. You will have encountered a range of experimental techniques for measuring rate constants and determining reaction orders, and a variety of theoretical tools - simple collision theory, the steady state approximation, transition state theory, to name a few - that can be used to interpret or even predict the experimental results.

A rate constant determined in a typical kinetics study is a highly averaged quantity, the aggregate outcome of an unimaginably large number of individual collisions between reactant molecules. In contrast, a chemical reaction dynamics study aims to understand chemistry at an exquisite level of detail by probing chemical reactions on the scale of single reactive collisions between molecules. As we shall see, it is possible to control the velocities, quantum states, and even the geometrical orientation of the colliding molecules and to measure the same properties in the products in order to understand the effect of each of these variables on the reaction under study. When we study chemistry at the single-collision level, we find that every chemical reaction bears its own unique fingerprint, embodied in the kinetic energy, angular distribution, and rotational and vibrational motion of the newly formed reaction products. These quantities reflect the forces acting during the reaction, particularly in the transition state region, and their measurement often provides unparalleled insight into the basic physics underlying chemical reactivity. Gaining an understanding of chemistry at the single collision level is the aim of this lecture course.

The first four lectures of this course will introduce most of the key concepts in reaction dynamics, including a detailed description of collisions, the concept of reactions occurring over potential energy surfaces, and an overview of experimental techniques used to probe single collision events. The final four lectures, which will be given by Mark Brouard, will develop these ideas in more detail and use them to explain the observed dynamics in a wide range of chemical systems.

1. COLLISIONS

Collisions lie at the very heart of chemistry. In the gas or liquid phase, a typical molecule undergoes billions of collisions every second. In this course, we will learn about the basic physics describing collisions, experiments and calculations that can be carried out to study them, and ways in which the results can be interpreted in order to learn about reaction mechanisms.

Collisions may be categorised into three types:

(i) Elastic collisions are collisions in which kinetic energy is conserved The collision partners have the same total translational kinetic energy after the collision as they did before the collision, and no energy is

transferred into internal degrees of freedom (rotation, vibration etc). Note that the kinetic energy of each individual collision partner may change, but the total kinetic energy remains constant.

(ii) Inelastic collisions are collisions in which kinetic energy is not conserved, and energy is converted between different forms e.g. translational to rotational or vibrational. Reactive collisions are a subset of inelastic collisions, but the term is usually used to describe collisions in which translational kinetic energy is transformed into internal excitation of one or both of the collision partners (or vice versa).

(iii) A *reactive collision* is a collision leading to a chemical reaction i.e. a collision in which chemical bonds are made or broken, so that the species leaving the collision region are chemically distinct from those that entered. The collision energy must be high enough to overcome any activation barrier associated with reaction. As noted above, reactive collisions are a special case of inelastic collisions.

Reactive collisions are the processes in which chemical change occurs, while inelastic collisions are often the means by which molecules gain enough energy to overcome activation barriers so that subsequent collisions may lead to reaction.

All collisions must obey certain physical laws, such as conservation of energy and both linear and angular momentum. There are also a number of concepts associated with collisions that will probably be less familiar, and which we will now explore.

1.1 Relative velocity

Rather than considering the individual velocities, $\boldsymbol{v}_1$ and $\boldsymbol{v}_2$, of the two collision partners, it is often more useful to consider their relative velocity. The relative velocity is simply the difference between the individual velocities, and corresponds to the 'apparent' velocity of the second particle to an observer travelling along with the first particle (or vice versa).

$$\boldsymbol{v}_{\text{rel}} = \boldsymbol{v}_1 - \boldsymbol{v}_2 \qquad (1.1)$$

Analogy: imagine you are sitting on a moving train and measuring the apparent velocity of a second train. If the second train is travelling in the same direction as your train (i.e. away from your train), it will appear to have a lower velocity than its true velocity, while if it is travelling in the opposite direction (i.e. towards your train) it will appear to have a higher velocity.

The relative velocity is very important in reaction dynamics, as it determines the collision energy, and therefore the probability of overcoming any energy barrier to reaction. To extend the 'train' analogy above, the collision energy is much lower when the two trains are travelling in the same direction (low relative velocity) than when they suffer a head-on collision (high relative velocity).

1.2 Collision energy, total kinetic energy, and conservation of linear momentum

The total kinetic energy of the colliding particles is simply equal to the sum of their individual kinetic energies:

$$K = \tfrac{1}{2} m_1 v_1^2 + \tfrac{1}{2} m_2 v_2^2 \qquad (1.2)$$

Where m_1 and m_2 are the masses of the two particles. Alternatively, the total kinetic energy can be broken down into a contribution associated with the velocity of the centre of mass of the collision partners, and a contribution associated with their relative velocity.

$$K = ½ Mv_{CM}^2 + ½ \mu v_{rel}^2 \quad (1.3)$$

where $M = m_1 + m_2$ is the total mass and μ the reduced mass of the two particles, v_{CM} is the velocity of the centre of mass of the particles, and v_{rel} is their relative velocity. The velocity of the centre of mass is calculated from

$$\boldsymbol{v}_{CM} = \frac{m_1\boldsymbol{v}_1 + m_2\boldsymbol{v}_2}{M} \quad (1.4)$$

The total linear momentum of the two particles must be conserved throughout the collision, and is equal to

$$\boldsymbol{p} = m_1\boldsymbol{v}_1 + m_2\boldsymbol{v}_2 = M\boldsymbol{v}_{CM} \quad (1.5)$$

(Note that Equations 1.4 and 1.5 are equivalent). Since the momentum of the centre of mass is conserved, the kinetic energy associated with the motion of the centre of mass, $K = ½ Mv_{CM}^2 = p^2/2M$, must also be conserved throughout the collision, and is therefore not available to overcome any energetic barriers to reaction. Only the kinetic energy contribution arising from the relative velocity of the two particles is available for reaction. This energy is known as the collision energy.

$$E_{coll} = ½ \mu v_{rel}^2 \quad (1.6)$$

Exercise: Prove that Equations (1.2) and (1.3) are equivalent.

1.3 Conservation of energy and energy available to the products.

The total energy must be conserved in any collision. Before the collision, the total energy is the sum of contributions from the kinetic energies of the collision partners (or, equivalently, the kinetic energies associated with their relative motion and the motion of their centre of mass) and any internal energy associated with rotation, vibration, or electronic excitation of the reactants. The reaction itself may consume energy (an endoergic reaction, with a positive $\Delta_r H$) or release energy (an exoergic reaction, with a negative $\Delta_r H$), and this must be taken into account when considering the amount of energy available to the products.

$$E_{avail} = E_{coll} + E_{int}(\text{reactants}) - \Delta_r H_0 \quad (1.7)$$

Note that DrH0 denotes the enthalpy of reaction at 0 Kelvin (i.e. for ground state reactants reacting to form ground state products). The energy available to the products may be distributed between translational and internal energy of the products.

1.4 Impact parameter, *b*, and opacity function, *P*(*b*)

The impact parameter quantifies the initial perpendicular separation of the paths of the collision partners. Essentially, this is the distance by which the colliding pair would miss each other if they did not interact in any way, and can be found by extrapolating the initial straight-line trajectories of the particles at large separations to the distance of closest approach.

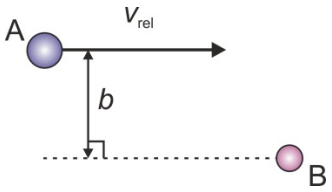

The probability of reaction as a function of impact parameter, *P*(*b*), is called the *opacity function*. Opacity functions will be covered in more detail later in the course.

1.5 Collision cross section, σ_c

You have come across the collision cross section before, in the context of simple collision theory (first and second year kinetics courses). The collision cross section is defined as the cross sectional area that the centres of two particles must lie within if they are to collide. We can use a very simple model to gain a conceptual understanding of the collision cross section. Consider the 'kinetic gas' model, in which there are no interactions between particles, and the particles act like hard spheres or 'billiard balls'. In the figure below, imagine that we have frozen the motion of all of the particles apart from the darker coloured particle positioned on the left in the side-on view, and in the foreground in the head-on view. We see that the moving particle will only collide with other particles whose centres lie within the cross sectional area $\sigma_c = \pi d^2$, where *d* is the particle diameter. We define the quantity σ_c as the collision cross section.

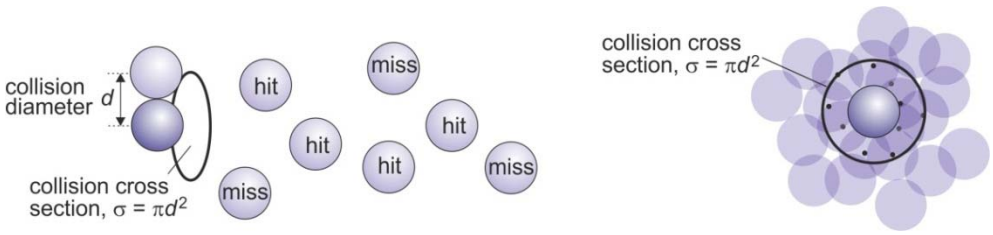

In the more general case of interacting particles, attractive interactions may mean that trajectories with impact parameters larger than the particle diameter, i.e. *b*>*d*, can lead to collisions. In this case the collision cross section will be somewhat larger than the hard-sphere collision cross section illustrated above.

1.6 Reaction cross section, σ_r

You have also come across the reaction cross section before in the context of simple collision theory. In that context, the reaction cross section is found by multiplying the collision cross section by a 'steric factor',

i.e. $\sigma_r = P\sigma_c$, which accounts for the fact that geometrical requirements mean that in general not all collisions lead to reaction. In this course we will treat the reaction cross section more rigorously.

The reaction cross section is the microscopic or single-collision version of a rate constant, and represents the reaction probability as an effective cross sectional area within which the two reactants must collide in order for reaction to occur. For a reaction between two species that can be modelled as hard spheres, so that the reaction probability is uniform for impact parameters between zero and some maximum value b_{max}, then the reaction cross section is

$$\sigma_r = \pi b_{max}^2 \tag{1.8}$$

More generally, the reaction cross section is given by integrating the reaction probability as a function of impact parameter and angle.

$$\sigma_r = \int_0^{2\pi} \int_0^{b_{max}} P(b)\, b\, db\, d\phi = 2\pi \int_0^{b_{max}} P(b) b\, db \tag{1.9}$$

The volume element $2\pi b db$ is illustrated below.

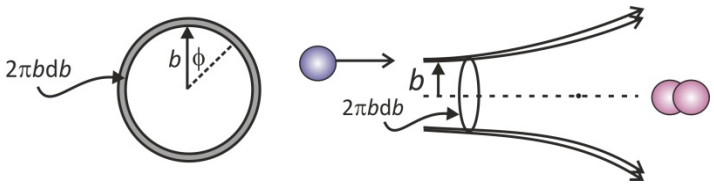

1.7 Excitation function, $\sigma_r(E_{coll})$

The excitation function quantifies the dependence of the reaction cross section on collision energy. It is the microscopic equivalent of the temperature dependence of the rate constant. Broadly speaking, there are two different types of excitation function, shown below, with the type exhibited by a particular reaction depending on whether or not the reaction has an activation barrier.

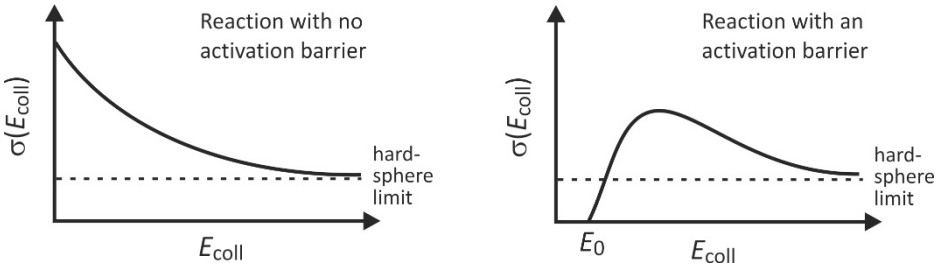

1. *Exoergic with no barrier*

This type of excitation function is typical of many exoergic[1] processes, e.g. ion-molecule reactions. At low energies there is enough time for long-range attractive interactions (van der Waals interactions, dipole interactions etc). to act on the particles and the cross section is large. If the long-range interactions are

[1] When talking about single reactive collisions, the terms *endoergic* and *exoergic* are used in place of *endothermic* and *exothermic*.

strong, even particles with large impact parameters can be pulled together by the attractive interactions and undergo a collision. As the collision energy increases, the particles fly past each other faster and their trajectories are deviated by a smaller amount by the attractive interactions. The cross section therefore reduces, until eventually there is no time for any attractive forces to act and the so-called 'hard-sphere limit' is reached. At this point the cross section is given by $\sigma = \pi d^2$, where $d=r_A+r_B$ is the sum of the particle radii. For many reactions the hard-sphere limit is very small, and the excitation function essentially tends to zero at very high energies.

2. *Endoergic or exoergic with a barrier.*
When the reaction has a barrier, no reaction occurs until there is enough energy available to surmount the barrier and the cross section is zero. The cross section then increases to a maximum in the region where attractive forces can act (c.f. Arrhenius equation for macroscopic rate constants), before decreasing again to the hard sphere limit at high energies for the same reasons as described above. The excitation function is the product of the decreasing ' barrierless' excitation function described above and an 'Arrhenius-type' function which rises once the activation barrier is surmounted.

In the second part of this course (taught by Prof. Brouard), you will be introduced to simple models that reproduce the key features of both types of excitation function. The models focus on explaining the shape of the low energy part of the excitation functions, which is relevant to the types of collision experiment most commonly carried out in the laboratory.

Once we know the excitation function, expressed as a function of collision energy or relative velocity, the thermal rate constant may be recovered. From simple collision theory, the rate constant for a given relative velocity is simply $k(v) = v\,\sigma_r(v)$. Integrating over the velocity distribution $P(v)$ of the molecules present in the sample yields the thermal rate constant.

$$k(T) = \int_0^\infty v\,\sigma_r(v)P(v)\,dv \qquad (1.10)$$

1.8 Scattering into a solid angle, Ω

An angle is often defined in terms of an arc of a circle; we talk about "the angle subtended by an arc", one radian is the angle subtended by an arc the same length as the radius, and there are 2π radians in a circle. By analogy, we can define the solid angle subtended by an area on the surface of a sphere, as shown in the diagram below.

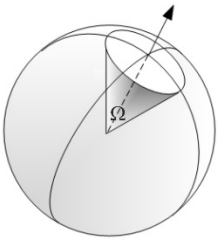

Solid angle is measured in units of steradians. One steradian is the solid angle subtended by an area r^2 on the surface of the sphere, and there are 4π steradians in a sphere.

In reaction dynamics, we need the concept of solid angle when considering the angular distribution of scattered products. The relative velocity vector of the reactants is an axis of cylindrical symmetry in the collision, with the consequence that scattering occurs symmetrically about this direction. When we refer to products being scattered at a given angle from the relative velocity vector, they are actually scattered into a cone rather than a single direction i.e. they are scattered into a solid angle rather than at a single angle.

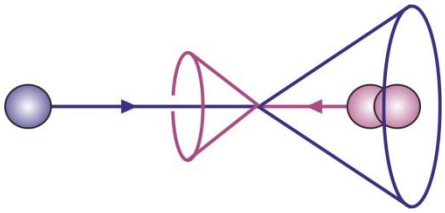

1.9 Differential cross section, $\frac{d\sigma}{d\Omega}$

Formally, the differential cross section (DCS) describes the probability of scattering into a given solid angle $d\Omega = \sin\theta d\theta d\phi$ between Ω and $\Omega+d\Omega$ in the centre of mass frame (see later). However, as noted above, scattering is symmetrical about the relative velocity vector of the collision partners, and so since there is no dependence on ϕ, it is often referred to as the probability of scattering at a given angle θ from the reactant relative velocity vector. The DCS therefore tells us the extent to which collision products are scattered forwards ($\theta = 0°$), backwards ($\theta = 180°$), or sideways ($\theta = 90°$) relative to the incoming collision partners. As we shall see, the DCS contains a great deal of information on reaction mechanisms, and differential cross sections will be considered in some detail later on in the course.

1.10 Orbital angular momentum, *L*, and conservation of angular momentum

In the context of a collision, the orbital angular momentum is an angular momentum associated with the relative motion of the collision partners as they approach and collide. **It is not to be confused with the quantum mechanical orbital angular momentum of an electron in an atomic orbital.** Even for two particles travelling in completely straight lines, there is an associated orbital angular momentum when their relative motion is considered. We can illustrate this by looking at the line of centres of the two particles at various points in their trajectory.

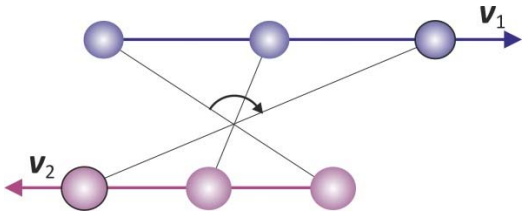

We see that even though the particles are travelling in straight lines, the line of centres of the particles rotates about their centre of mass. Only head on collisions with an impact parameter b=0 have no associated orbital angular momentum.

Mathematically, the orbital angular momentum for a colliding pair of particles is given by

$$\boldsymbol{L} = \boldsymbol{r} \times \boldsymbol{p} \qquad (1.11)$$

where **r** is the (vector) separation of the particles and ***p*** is their relative linear momentum. We can therefore find the magnitude of ***L*** from

$$|\mathbf{L}| = |\mathbf{r} \times \mathbf{p}| = |\mu\, \mathbf{r} \times \mathbf{v}_{rel}| = \mu\, v_{rel}\, r \sin\theta \qquad (1.12)$$

where θ is the angle between r and $\boldsymbol{v}_{rel}$. At large separations, $r\sin\theta$ is simply equal to the impact parameter, b, giving

$$|\boldsymbol{L}| = \mu v_{rel} b \qquad (1.13)$$

Because the total angular momentum (the sum of the orbital angular momentum ***L*** and any rotational angular momentum ***J*** of the collision partners) must be conserved throughout the collision, this is true right up until the point that the particles collide, assuming the rotational states of the particles do not change.

In the products, the total angular momentum, ***L*** + ***J***, must be the same as before the collision, but angular momentum can be exchanged between ***L*** and ***J*** during the collision.

2. POTENTIAL ENERGY SURFACES

The previous section provided an introduction to some of the basic physics of atomic and molecular collisions. However, it gave us no insight into why some collisions simply lead to elastic scattering, while others lead to energy transfer or even chemical reaction. When inelastic and reactive collisions are studied in even more detail, we find that they often lead to preferred scattering in a particular direction, or that they populate specific rotational, vibrational, and electronic quantum states of the products, or that the outcome of the collision depends strongly on the initial kinetic energies, quantum states, or relative orientations of the reactants. To explain all of these observations, we need the concept of a potential energy surface. We will start by considering a simple 'one dimensional' potential energy surface, namely the interaction potential between two atoms.

2.1 The interaction potential and its effect on the collision cross section

We have discussed the effect of atomic and molecular interactions on reaction cross sections in a qualitative way in Section 1.7, in the context of excitation functions. There we introduced the idea that attractive interactions between the colliding particles could increase the cross section above what we would expect for a 'hard sphere' collision. Here we provide a somewhat more quantitative treatment in the context of collision cross sections.

The potential energy of a colliding pair of atoms depends on a single coordinate, namely their separation. The simplest model is the hard sphere potential, in which there is no interaction until the two spheres touch. The maximum impact parameter is $b_{max} = d = r_1 + r_2$, the sum of the radii, and the collision cross section is $\sigma_c = \pi b_{max}^2$. The cross section is not energy dependent. The interaction potential, an example collision trajectory, and the cross section for such a system are shown below.

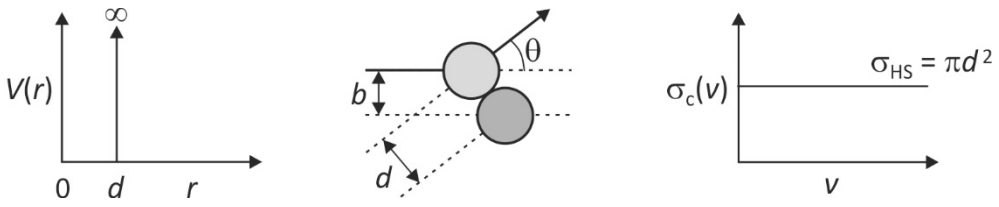

In contrast, a realistic interatomic potential has a long-range attractive component and a short-range repulsive component. Often, the Lennard-Jones potential is used, which has a repulsive component proportional to $1/r^{12}$ and an attractive component proportional to $1/r^6$.

$$V(r) = \varepsilon\left(\left(\frac{r_0}{r}\right)^{12} - 2\left(\frac{r_0}{r}\right)^{6}\right) \qquad (2.1)$$

Here ε is the depth of the potential well at the minimum, and r_0 is the particle separation at the minimum. The potential is shown below, together with an example collision trajectory and collision cross section. In contrast to the hard sphere potential, the impact parameter can now exceed d due to the attractive interaction between the particles. The two particles are attracted to each other as they approach, but are then scattered before actually touching by the repulsive part of the potential.

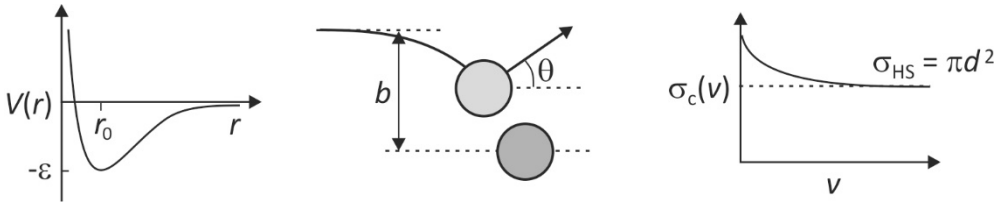

Landau, Lifshitz and Schiff proposed an expression to relate the collision cross section to the Lennard-Jones parameters ε and r_0 and to the relative velocity v of the colliding particles.

$$\sigma_c(v) = 8.083\left(\frac{2\varepsilon r_0^{\,6}}{\hbar v}\right)^{2/5} \qquad (2.2)$$

Note that the $1/v^{2/5}$ dependence yields a function similar to that introduced in the excitation function for reactions without a barrier, which we met in Section 1.7.

We see already that the collision cross section depends on the interactions between the colliding particles, and therefore that measurement of the collision cross section can provide information about these interactions. As we shall discover in the following sections, these interactions in fact completely determine every aspect of the collision dynamics.

2.2 Atomic and molecular interactions

More realistic potentials take into account all of the various types of atomic and molecular interactions that can contribute to the attractive part of the interaction potential. The various contributions can all be written in the form

$$V(r) = -\frac{a}{r^n} \qquad (2.3)$$

where a is a constant that depends on quantities such as the atomic or molecular charge, dipole moments, polarisabilities etc, and n depends on the type of interaction:

- $n = 1$ Ion-ion interaction
- $n = 2$ Ion-dipole interaction
- $n = 3$ Dipole-dipole interaction
- $n = 4$ Ion-induced dipole interaction
- $n = 5$ Dipole-induced dipole interaction
- $n = 6$ Induced dipole-induced dipole interaction (also known as van der Waals, London, or dispersion interaction)

2.3 The potential energy surface (PES) for a polyatomic system

For a collision between two atoms, we have seen that the potential energy depends on a single parameter, the internuclear separation. When two molecules collide, there are many more degrees of freedom, associated with the positions of each of the individual atoms, all of which may be important in determining the outcome of a collision. The figure below shows the way in which the number of degrees of freedom increases with the number of atoms in the system. Specifying the relative position of two atoms requires a single coordinate; for three atoms we require two interatomic distances and an angle; for four atoms we require three interatomic distances, two bond angles, and a dihedral angle, and so on[2].

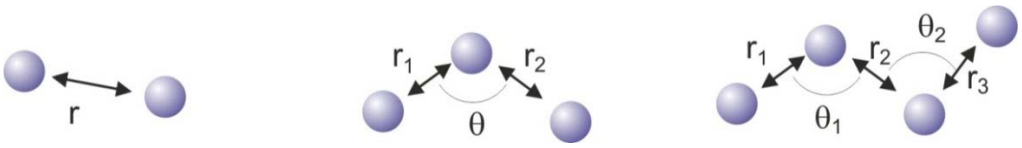

The result is that to describe the potential energy, we have to move from a potential energy *curve* to a potential energy *surface*. The potential energy surface quantifies the potential energy of the system as a function of all (or some) of the nuclear coordinates of the atoms involved, or in terms of bond lengths, bond angles etc. Each point on the surface corresponds to a particular geometrical configuration of atoms, and there may be several potential energy surfaces corresponding to different possible electronic states of the system. This is shown schematically below.

[2] The total number of coordinates required to describe the positions of N atoms is 3N. However, the energy of the system depends only on the relative coordinates of the atoms. These are not changed by a translation of the whole system or by rotation of the whole system, each of which require 3 of the 3N degrees of freedom, so the total number of coordinates required is 3N-6 (or 3N-5 for a linear system, in which only two degrees of freedom are needed to describe a rotation of the whole system).

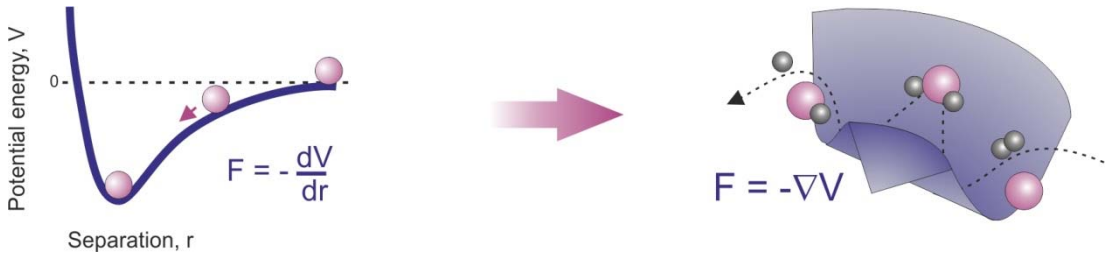

2.4. The PES and the collision dynamics

If you cast your mind back to the first year 'Physical Basis of Chemistry' lecture course, you may recall that if the potential energy of a system is known, the force acting on the system may be determined from the first derivative or gradient of the potential. For a potential energy function that depends on a single coordinate, we have

$$F(r) = -\frac{\mathrm{d}V(r)}{\mathrm{d}r} \tag{2.4}$$

while for a potential energy function that depends on coordinates r_1, r_2, r_3 etc, we have[3]

$$\boldsymbol{F} = -\nabla \mathrm{V} = -\left(\frac{\partial V}{\partial r_1}\frac{\partial V}{\partial r_2}\frac{\partial V}{\partial r_3}\ldots\right) \tag{2.5}$$

The gradient of the potential energy surface therefore determines the forces acting on all of the atoms, and thereby determines their subsequent motion. The potential energy surface (together with the initial conditions – whereabouts on the surface the system starts, and how much kinetic energy it has) therefore completely defines the reaction dynamics. Conceptually, we can think of the dynamics in terms of 'rolling a ball' over the potential energy surface, as shown schematically in the figure above. As the ball rolls over the surface, different atomic configurations are sampled, allowing us to reconstruct a 'movie' of the collision dynamics. We can of course be much more rigorous than this, and can calculate the trajectory of the system mathematically. Starting from a particular point on the potential energy surface corresponding to the initial positions of the atoms, we calculate the gradient of the surface, and therefore the forces acting on the atoms. We then solve Newton's third law of motion to determine the trajectory, $\boldsymbol{r}(t)$, of the system i.e. the way in which the atomic positions evolve as a function of time

$$\boldsymbol{F} = m\boldsymbol{a} = m\frac{\mathrm{d}^2\boldsymbol{r}}{\mathrm{d}t^2} \tag{2.6}$$

We allow the system to follow this trajectory for a short period of time until it has reached a new point on the surface. We must then find the gradient again to determine an up to date set of forces, solve to find the new trajectory, let the system follow this trajectory for a short period of time to reach a new position on the surface, and so on. This procedure is known as a *classical trajectory* calculation, and with some modifications to take account of the quantised energy levels of the system, the approach may be used to

[3] Applying the gradient operator, $\nabla = \left(\frac{\partial}{\partial r_1}\frac{\partial}{\partial r_2}\frac{\partial}{\partial r_3}\ldots\right)$, to the potential yields the force vector, with components of force along the coordinates r_1, r_2, r_3 etc.

predict virtually all of the experimental observables associated with a collision, including the identity of the products, their speed and angular distributions, and their quantum state populations.

Alternatively, we can carry out fully quantum mechanical calculations to study the dynamics. This approach involves constructing an initial wavefunction for the system and propagating it across the potential energy surface by solving the time-dependent Schrodinger equation.

2.5 Construction of the PES

In order to calculate a point on the potential energy surface, we need to solve the Schrodinger equation to determine the energy at the atomic configuration of interest. While it is not possible to solve the Schrodinger equation exactly, there are numerous electronic structure software packages (e.g. Gaussian, Gamess, MolPro) which can solve the equation numerically to a high degree of accuracy. In principle, to construct the complete PES we would need to solve the Schrodinger equation for every possible atomic configuration. In practice, we solve the Schrodinger equation for a reasonable number of configurations and then fit the data points to a suitable function in order to generate a smooth surface. Though this procedure is straightforward in principle, the construction of an accurate potential energy surface for a chemical system is a challenging problem, which quickly becomes intractable as the number of atoms in the system, and therefore the number of degrees of freedom required, increases. Nonetheless, accurate surfaces are available for a considerable number of reactive chemical systems, and comparing the predictions of these surfaces with the results of experimental measurements provides a stringent test both for theory and experiment. Note that the construction of potential energy surfaces assumes the Born-Oppenheimer approximation, i.e. that the electronic and nuclear motion can be decoupled, so that it is valid to calculate the electronic energy at a series of fixed nuclear geometries.

We shall now look at some examples of different types of potential energy surfaces and the consequences for the corresponding scattering processes.

2.6 The potential energy surface for a linear triatomic system

Consider a reacting system of three atoms, i.e. A + BC $\rightarrow$ AB + C. For simplicity, we will constrain the atoms to lie in a straight line throughout the reaction. This allows the relative positions of all three atoms to be defined by two distances, r_{AB} and r_{BC}, and the potential energy surface for the reaction is therefore a function of these two coordinates. To begin constructing the potential energy surface, we consider the interaction between the atoms in the *entrance channel* of the reaction i.e. before the reactive collision, as the A atom approaches the BC molecule. If we fix the r_{BC} distance, there will be a long-range attractive interaction between A and BC, and a short range repulsive interaction, and the potential energy curve will look something like that shown in the figure below. The figure represents a *cut* through the full potential energy surface, $V(r_{AB},r_{BC})$ for a fixed value of r_{BC}. The picture would be similar if we looked at the exit channel of the reaction i.e. if we fixed the AB distance and plotted the interaction potential energy as a function of r_{BC}.

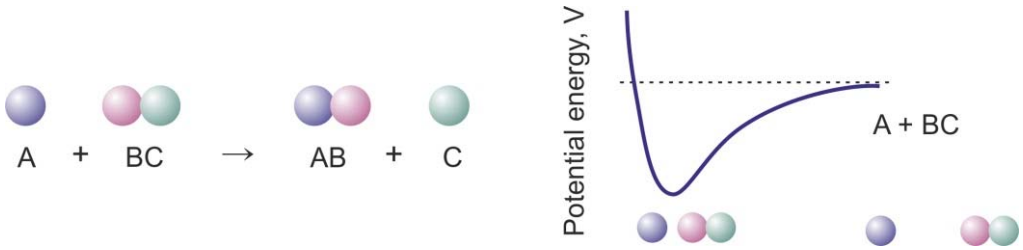

By considering the energy of the system at various A-B-C separations, we now know enough about molecular interactions to be able to predict the form of the complete potential energy surface. The short-range repulsive interactions mean that the energy will be high when either or both of the r_{AB} and r_{BC} distances are very small, and the energy will be lowest when r_{AB} and/or r_{BC} are at their equilibrium distance (corresponding to the minimum in the curve above). The energy increases again as we move out to large separations where there are no attractive interactions between the atoms. The resulting potential energy surface is shown below as a contour plot (on the left) and as a 3D plot (on the right). The surface resembles a curved 'half pipe'; keen skateboarders or snowboarders might be familiar with analogous gravitational potential energy surfaces of this form.

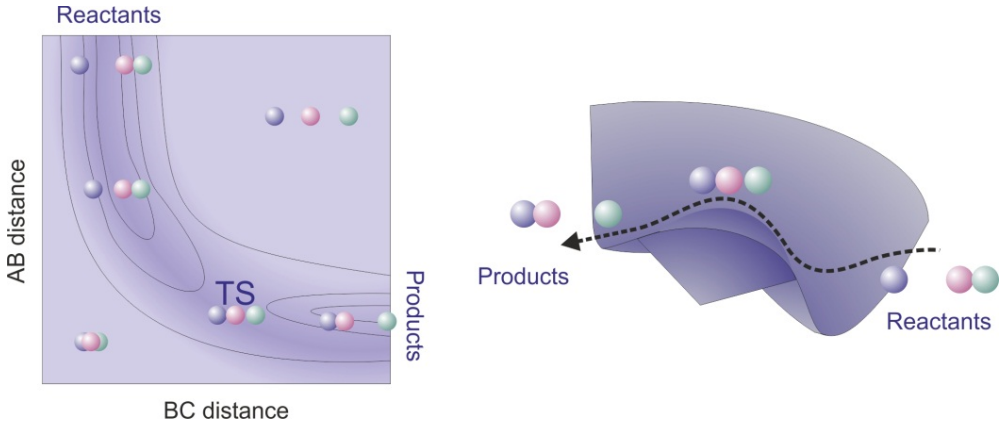

The minimum energy path across the surface follows the base of the 'half pipe', and is known as the *reaction coordinate*. Note that the transition state appears as a 'hump' along the reaction coordinate, which the reactants must surmount to form products. As shown below, if we plot the potential energy along the reaction coordinate, we recover the familiar reaction potential energy profile.

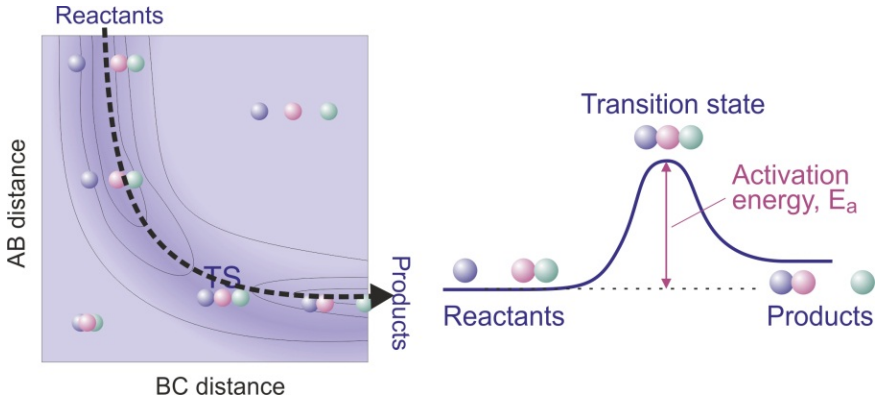

2.7 Reactive and non-reactive trajectories across the potential energy surface

As noted earlier, the outcome of a collision depends both on the shape of the potential energy surface and on the initial velocities and internal states of the reactants. In this section we will consider a few example trajectories across a surface similar to that constructed in Section 2.6 above, again for an A + BC → AB + C reaction. The four trajectories we will consider are shown below.

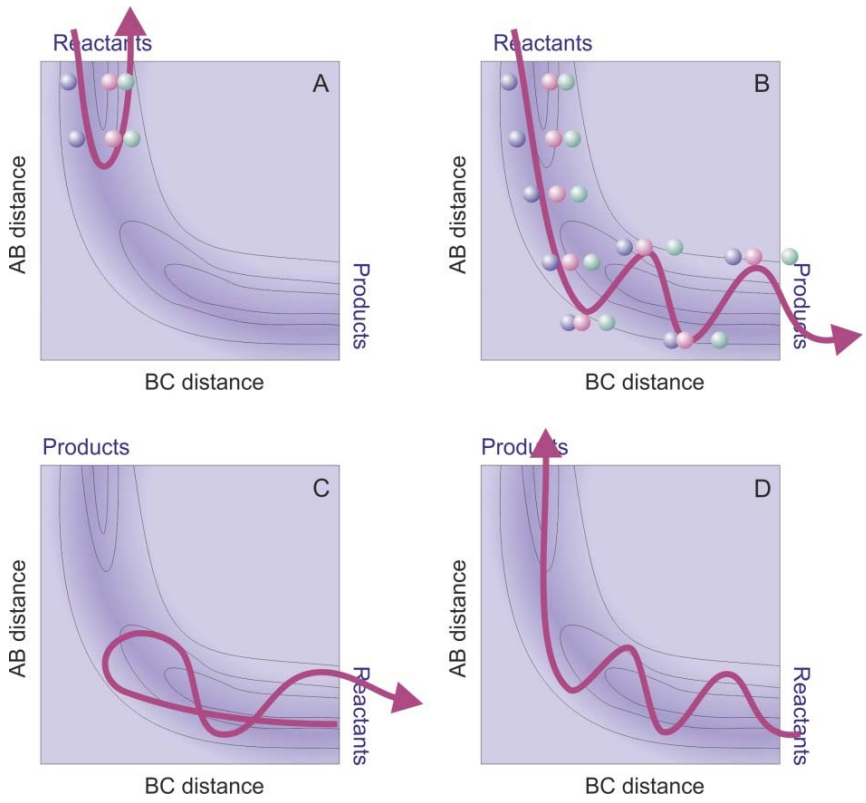

A. The reactants are launched onto the surface with a low relative velocity. They have insufficient kinetic energy to surmount the activation barrier, and the trajectory 'turns round' and returns along the entrance channel to the reactants. Such a trajectory corresponds to elastic or inelastic scattering, depending on whether or not there is a change in rotational or vibrational state of the diatomic reactant.

B. The reactants are launched onto the surface with a high relative velocity. They have sufficient energy to surmount the activation barrier, and at small AB distances they eventually roll up the repulsive wall of the surface, before rolling back down again and following an oscillating trajectory out into the product channel. Note that as atom C departs, the AB distance periodically extends and contracts, corresponding to vibration of the AB product.

From this simple consideration of two trajectories, we have therefore been able to predict that in order for reaction to occur on this potential energy surface, we need a significant amount of energy in relative translational motion of the reactants, and that some of this energy is converted into vibrational motion of the products. This is a fairly common observation, which you will return to in the second half of this lecture course under the heading of 'Polanyi's rules'.

Trajectories C and D correspond to the reverse reaction, AB + C → A + BC

C. Trajectory C is another unsuccessful trajectory. The reactants have a reasonably high relative velocity in this case, but the position of the barrier in the exit channel for the reverse reaction means that the trajectory merely 'glances' off the barrier and returns along the entrance channel to reactants. In this case, we can see that some of the translational energy of the incoming reactants is converted into vibration of the AB molecule following the collision; this is therefore an inelastic scattering trajectory.

D. In this trajectory the reactants begin with a mixture of translational and vibrational kinetic energy, and the trajectory successfully surmounts the barrier to form products with no vibrational excitation.

2.8 General features of potential energy surfaces

The simple potential energy surfaces we have considered so far consist of reactant and product 'valleys' separated by a transition state. In general, potential energy surfaces can be much more complicated than this, particularly for larger chemical systems. In the diagram below, we define a number of different topological features that may be found on a reaction potential energy surface. The diagram is taken from a chapter on 'Geometry Optimisation' in the Encyclopedia of Computational Chemistry (John Wiley and Sons, Chichester, 1998, p 1136-1142). There are several features to note:

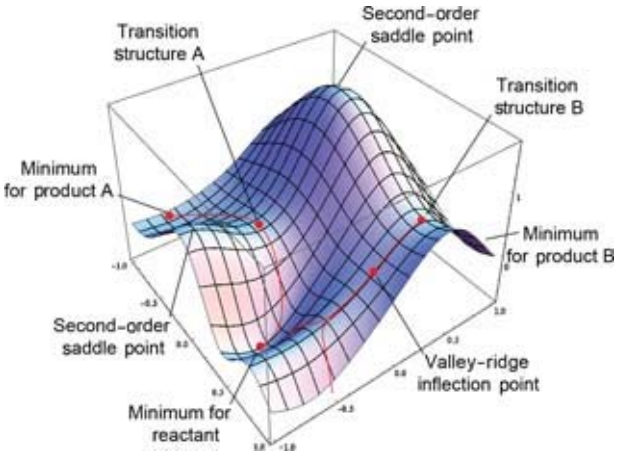

(i) Stable species appear as minima on the potential energy surface, with the deepest wells corresponding to the most stable species. Reactants and products tend to appear as fairly deep minima on the surface, while intermediates will have shallower well depths.

(ii) Transition states appear as saddle points on the surface. A saddle point(sometimes called a first-order saddle point) is a maximum in one dimension and a minimum in all other dimensions, and as the name suggests, is similar in shape to a horse's saddle.

(iii) Other structures, such as second-order saddle points (a maximum in two dimensions and minimum in all others) and ridges, can also appear, but we will not look at these in any detail in this course.

2.9 Examples of potential energy surfaces for real chemical systems

We will now look at some examples of potential energy surfaces for a few bimolecular reactions and photoinitiated events. Some of these processes involve more than one electronic state, and therefore more than one potential energy surface. As we will see, population can be transferred between different potential energy surfaces, opening up numerous possibilities for the reaction dynamics relative to processes occurring on a single surace.

(i) ***The simplest chemical reaction: H + H_2 → H_2 + H***

[Figure adapted from *Science,* 331 411-412 (2011)]

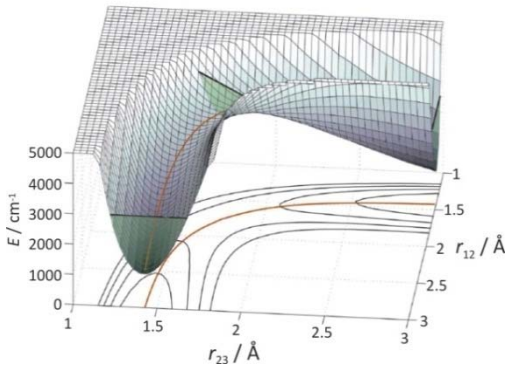

The simplest chemical reaction, constrained to react in a linear geometry, has a perfectly symmetrical potential energy surface, with the transition state in the centre of the curve of the 'half pipe'. The figure shows the surface in 3D view and in contour view, with the reaction coordinate superimposed onto both views.

(ii) ***Photodissociation of NO_2***

[Figure adapted from *Science*, 334 208-212 (2011)]

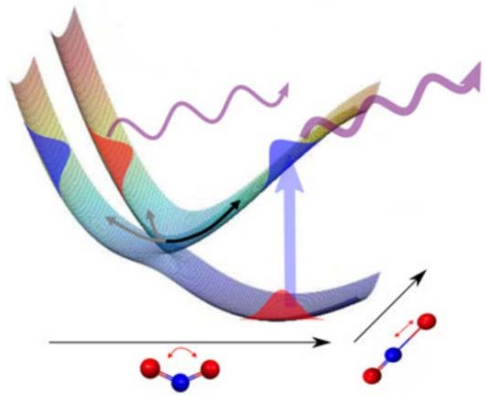

The figure shows the ground and first electronically excited states for the NO_2 molecule, plotted as a function of the bond angle and one of the NO bond lengths (the second NO bond is held fixed). We can use the surfaces to understand the dissociation dynamics following absorption of a photon. Note that this process does not involve any collisions, though photodissociation is sometimes referred to as a 'half collision'. In NO_2, the equilibrium geometry for the excited state is much more bent than for the ground state, so following excitation the molecule bends to reduce its energy. The excited and ground states cross at a conical intersection, allowing the wavefunction to funnel through the conical intersection back to highly excited vibrational levels of the ground state, from which it dissociates. The bent geometry from which dissociation occurs leads to a high degree of rotational excitation in the diatomic fragment, since the N atom receives a strong 'kick' when the N-O bond dissociates.

(iii) ***Photoinduced cis-trans isomerisation in retinal***

[Figure adapted from *Conical Intersections*, edited by W. Domcke, D. R. Yarkony, and H. Koppel, (World Scientific, Singapore, 2003)]

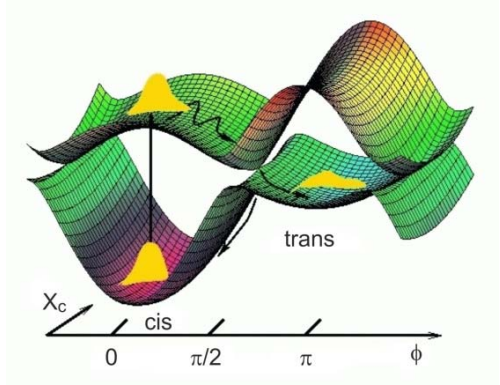

Rhodopsin is a protein that is intimately involved in human vision and consists of a protein moeity, opsin, with a covalently bound cofactor, 11-cis-retinal. Absorption of light by retinal leads to rapid cis-trans isomerisation, inducing a conformational change in the opsin, which triggers a sequence of events leading to visualisation of the light by the brain. The potential energy surfaces give us insight into the dynamics of the cis-trans

isomerisation. On absorption of a photon, the 11-cis retinal is excited to a higher-lying electronic state. The excited state can lower its energy by undergoing torsion about the double bond, with the equilibrium geometry lying at an angle of 90 degrees. At this point population can funnel back down to the ground state through a conical intersection and equilibrate further to yield ground-state all-trans retinal.

(iv) ***H + CO_2 → OH + CO***

[Figure adapted from *Acc. Chem. Res.*, 43 1519 (2010)]

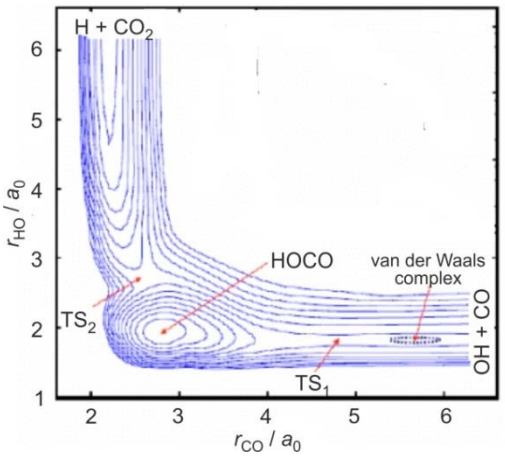

In contrast to the systems we have considered so far, the H+CO_2 reaction has a deep well on its potential energy surface corresponding to the relatively stable molecule HOCO. This leads to very different collision dynamics. Unlike the direct dynamics we have considered so far, in which molecules collide, exchange atoms, and separate in essentially a single concerted step, when a deep well is present on the surface the system can become trapped in the well for significant amounts of time. As we shall see in later lectures, direct reactions often lead to strongly anisotropic angular distributions. In contrast, when a long-lived complex forms and survives for multiple rotational periods, all 'memory' of the initial approach directions of the reactants are lost, and an isotropic angular distribution results. The energy available to the system also has time to become distributed statistically amongst the various modes of motion of the complex, leading to characteristic 'statistical' population distributions in the reaction products. In contrast, the newly formed (or 'nascent') products of direct reactions often have highly non-statistical quantum state distributions.

(iv) ***OH + SO → H + SO_2***

[Figure adapted from *Chem. Phys. Lett.*, 433(4-6) 279-286 (2007)]

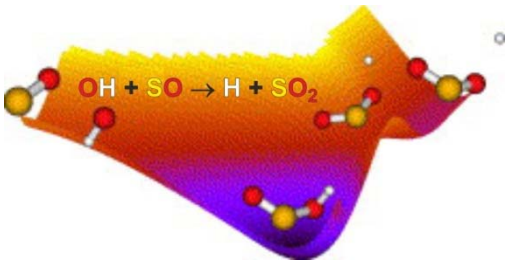

As we might expect, the situation is similar for the H + SO_2 reaction, in which the carbon atom has been replaced by sulphur. In this 3D view of the potential energy surface, the deep well corresponding to the HOSO complex is very clearly seen.

2.10 Mass weighted coordinates and the skew angle

The picture we have of 'rolling a ball' or point mass across a potential energy surface has so far worked very well in giving us a conceptual understanding of the reaction dynamics. However, when we examine this approach in a little more detail we find that this is something of an oversimplification. We will demonstrate the problem (and how to solve it) using the triatomic A + BC system we have already considered in some

detail. For this type of system it turns out that the appropriate mass for the 'rolling ball' is simply the reduced mass of the two reactants.

$$\mu = \frac{m_A m_{BC}}{m_A + m_{BC}} \qquad (2.7)$$

If we choose a coordinate system (r_{AB}, r_{BC}, θ) to define the relative positions of A, B and C, and restrict the atoms to be colinear ($\theta = \pi$) for simplicity, then we can write the total (kinetic plus potential) energy as follows.

$$E = \frac{1}{2}\left(\mu \dot{r}_{AB}^2 + 2\frac{m_A m_C}{M}\dot{r}_{AB}\dot{r}_{BC} + \mu' \dot{r}_{BC}^2\right) + V(r_{AB}, r_{BC}, \theta = \pi) \qquad (2.8)$$

where μ and μ' are the reduced masses of the reactants and products, M is the total mass, and $\dot{r} = \frac{dr}{dt}$.

We immediately see a problem. Using the (r_{AB},r_{BC}) coordinate system, the kinetic energy has a cross term in $\dot{r}_{AB}\dot{r}_{BC}$, and there are two different mass factors appearing in the terms in $\dot{r}_{AB}^2$ and $\dot{r}_{BC}^2$. The kinetic energy is not of the simple form $K = \frac{1}{2}\mu v^2$, and we cannot think of the motion as that of a single particle of mass μ moving across the surface. However, we can rescue the situation if we define a new set of coordinates called Jacobi coordinates, defined in the diagram below.

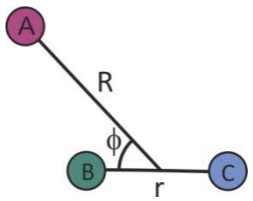

r = BC distance
R = distance from A to centre of mass of BC
ϕ = angle between r and R

Using these new coordinates, the expression for the total energy becomes

$$E = \frac{1}{2}\mu\left(\dot{R}^2 + \alpha^{1/2}\dot{r}^2\right) + V(R,r,\gamma=0) \qquad (2.9)$$

where $\alpha = \mu_{BC}/\mu$, with $\mu_{BC} = m_B m_C/m_{BC}$. The kinetic energy now does have the required simple form

$K = \frac{1}{2}\mu(v_x^2 + v_y^2) = \frac{1}{2}\mu v^2$, and we find that the picture of a particle of mass μ rolling over the potential energy surface is in fact correct, *so long as* we plot the surface with the following *mass weighted coordinates*.

$$x = R = r_{AB} + \frac{m_C}{m_{BC}} r_{BC}$$

$$y = \alpha^{1/2} r = \alpha^{1/2} r_{BC} \qquad (2.10)$$

Since x and y are simply linear combinations of our original axes r_{AB} and r_{BC}, this turns out to be equivalent to plotting the PES using the (r_{AB}, r_{BC}) axis system, but with the axes at an angle β instead of at 90 degrees to each other. The angle β is known as the skew angle, and is given by

$$\cos^2\beta = \frac{m_A m_C}{m_{AB} m_{BC}} \qquad (2.11)$$

When either A or C are light atoms (i.e. light attacking or departing atom), $\cos^2\beta$ is small, β is close to 90 degrees, and the dynamics are essentially as our original simple picture would predict. However, in other cases the skew angle can be quite small, leading to significantly different dynamics. The figure below shows a skewed axis system together with a typical trajectory. The simple picture developed above of kinetic energy being released into translational or vibrational motion in the products become more complicated in such cases.

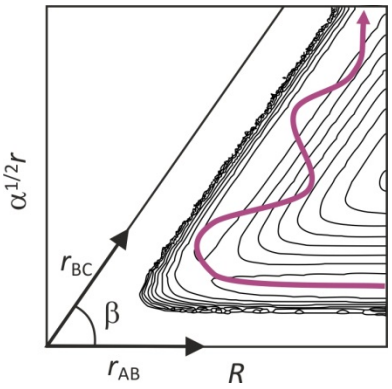

2.11 Orbital angular momentum, centrifugal barriers and the effective potential

In Section 1.8 we defined the orbital angular momentum of a colliding system, and noted that orbital angular momentum is conserved during a collision. Consider again the particle trajectory shown in Section 1.10 and reproduced below.

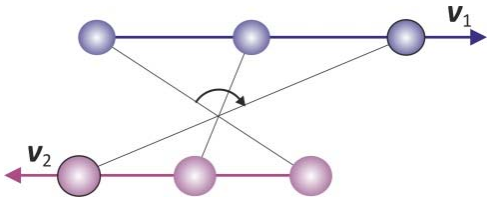

The relative kinetic energy of the two particles, $\frac{1}{2}\mu v_{rel}^2$, can be expressed as a sum of translational kinetic energy directed along the line of centres of the two particles and rotational kinetic energy associated with the orbital motion described above, i.e.

$$K_{rel} = \tfrac{1}{2}\mu v_{rel}^2 = \tfrac{1}{2}\mu \dot{r}^2 + \frac{L^2}{2\mu r^2} \qquad (2.12)$$

Only the component of the kinetic energy associated with motion along the line of centres is available to help overcome an activation barrier to reaction. The kinetic energy associated with the orbital motion is not available to help surmount an activation barrier, and because it has the effect of reducing the available energy, this term is often referred to as a *centrifugal barrier*. The centrifugal barrier term is often combined with the potential energy surface to give an effective potential. i.e.

$$V_{\text{eff}}(r) = V(r) + \frac{L^2}{2\mu r^2} \qquad (2.13)$$

As shown in the figure below, the centrifugal barrier can give rise to an effective barrier to reaction, even when the potential energy surface itself has no barrier.

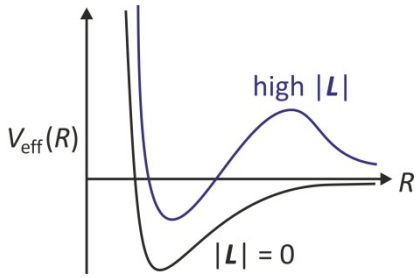

Using $L^2 = \mu^2 v_{\text{rel}}^2 b^2$ (see section 1.8), we can rewrite the effective potential as

$$V_{\text{eff}}(r) = V(r) + \frac{1}{2}\frac{\mu v_{\text{rel}}^2 b^2}{r^2} \qquad (2.14)$$

We see that the barrier will be largest for heavy systems at large impact parameters. The centrifugal barrier often has the effect of reducing the maximum impact parameter that can lead to successful reaction, thereby reducing the reaction cross section.

3. EXPERIMENTAL METHODS

3.1 Experimental aims

The 'ultimate' experiment in reaction dynamics would determine the cross section, velocity distribution, quantum state distribution, and any angular momentum polarisation for the products of a collision in which every property of the reactants (velocity, quantum state, etc) was specified. In practice, we aim for the most detailed observations we can make for comparison with theory. Measurable properties include:

(i) Total reaction cross sections at specified collision energies;

(ii) Product velocity (speed and angular) distributions;

(iii) Product internal state distributions;

(iv) Product alignment and/or orientation i.e. polarisation of angular momentum

(v) Dependence of the reaction on the orientation or alignment of the reactants.

In the following, we will explore some of the experimental techniques that have been developed to achieve these goals.

3.2 Isolating single collision events: temporal and spatial isolation

In order to obtain information about single collision events, the products must be detected before undergoing further collisions. Secondary collisions can change the velocities, internal states, and even the chemical identities of the collision partners, thereby destroying information on the properties of the nascent product molecule of interest. Eventually, secondary collisions lead to complete thermalisation of the reaction products, as is the case in a bulk kinetics experiment.

Isolating single collision events can be achieved using either of two approaches, known as *spatial isolation* and *temporal isolation*, respectively:

(i) In temporal isolation, we ensure that the mean time between collisions is longer than the time required to detect the reaction products. The mean time t between collisions is simply the inverse of the collision frequency, z (see first year Properties of Gases and Kinetics courses)

$$t = \frac{1}{z} = \frac{1}{\sigma_c \bar{v} n} \qquad (3.1)$$

where σ_c is the collision cross section, $\bar{v}$ is the mean relative velocity, and n is the number density of the gas. An example of an approach to studying single collisions that relies on temporal isolation is the laser pump-probe experiment. A first, 'pump', laser pulse is used to initiate reaction, and after a short delay (of anything from tens of femtoseconds up to a few tens of nanoseconds, depending on the type of experiment), a second 'probe' laser pulse is used to characterise the products formed via any one of a range of spectroscopic techniques. The 'measurement time' is determined by the pump-probe delay. For comparison, the time between collisions for N_2 gas at atmospheric pressure and 298 K is around 1 ns. Reducing the pressure readily allows temporal isolation to be achieved.

(ii) In spatial isolation, we ensure that the mean free path λ of the molecules is much larger than the distance the products must travel before they are detected. Spatial isolation is appropriate for experiments in which the products are detected through interaction with a physical detector, rather than spectroscopically through interaction with light. The mean free path is given by

$$\lambda = \bar{v} t = \frac{1}{\sigma_c n} \qquad (3.2)$$

An example of an experiment employing spatial isolation is the crossed molecular beam experiment, which we will consider in detail later. Crossed beam experiments are carried out under high vacuum conditions. In the 'classical' crossed beam experiment, collisions occur at the intersection between two molecular beams, and the products must fly from the crossing region to the inlet of a mass spectrometer to be detected.

3.3 Control of initial velocities

3.3.1. Molecular beams

Using beams of molecules provides a sample with a well-defined velocity distribution, and allows directional properties of chemical processes to be studied. There are two types of molecular beam sources,

known as effusive and supersonic sources, respectively. Both types of source work by allowing gas to escape from a high pressure region through a small orifice into a vacuum. The flow characteristics of the source are determined by the ratio of the mean free path in the source to the diameter of the orifice, a quantity known as the Knudsen number.

$$K_n = \frac{\lambda}{\phi} \qquad (3.3)$$

In an effusive source the diameter of the hole is smaller than the mean free path in the gas ($K_n > 1$), and in a supersonic source it is larger ($K_n < 1$). The orifice size is generally similar in the two types of source, but the supersonic source operates at a much higher gas pressure, giving a much shorter mean free path than in the effusive source. The two types of beam have very different properties.

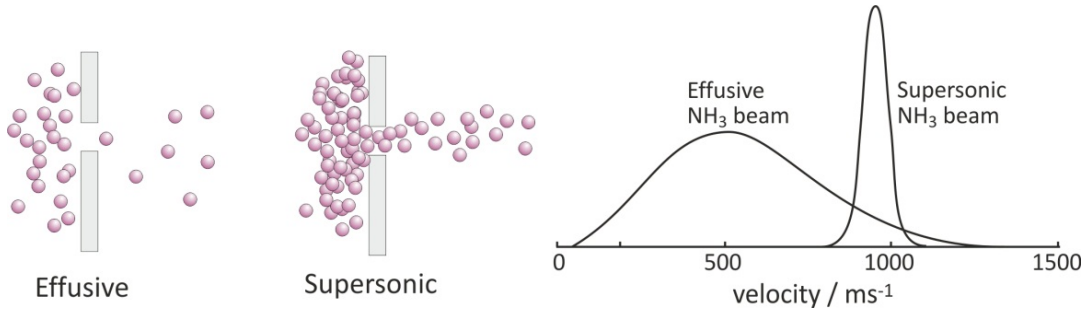

(i) Effusive sources

In an effusive beam, since molecules effectively 'wander' out of the hole whenever they 'collide' with it, the Maxwell-Boltzmann distribution of the molecular speeds in the source is more or less maintained in the molecular beam. The distribution is actually somewhat skewed towards higher velocities, since molecules with higher speeds undergo more collisions with the walls and are therefore more likely to exit the hole. The velocity components are conserved in the molecular beam, with the result that the beam has a broad $\cos^2\theta$ angular distribution, where θ is the angle between the molecular velocity and the beam axis (i.e. the direction normal to the wall of the chamber containing the hole). Effusive sources generally contain the gas at a low pressure, and are mainly only used to produce beams of metal atoms or other species that can only be prepared at low pressure in the gas phase. Usually the source is heated to high temperatures in order to obtain as high a vapour pressure as possible.

(ii) Supersonic sources

In supersonic sources, because the mean free path is much smaller than the diameter of the hole, many collisions occur as the molecules exit the hole and in the region immediately beyond it. Collisions that impart a velocity component along the beam axis are most successful at allowing a molecule to escape this region, with the result that the molecules that end up in the beam are those for which the collisions have converted almost all of their random translational energy and internal (rotational and vibrational) energy into directed translational kinetic energy along the beam axis. The beam molecules therefore have almost no internal energy, occupying only very low rotational quantum states, and have a very narrow speed distribution. The angular distribution about the beam axis is also much narrower than for an effusive beam. Since the width of the molecular speed distribution determines the temperature of a gas, by this

definition the molecules in a supersonic molecular beam are extremely cold. It is fairly standard to reach temperatures as low as 5 K by this very simple technique of expanding a gas through a small hole. At these low temperatures, only a few low-energy rotational states are occupied.

The maximum or terminal velocity of molecules in a supersonic beam can be determined by assuming that all of the internal energy of the molecules inside the source is converted into kinetic energy directed along the beam axis, in an *isenthalpic* expansion (i.e. $\Delta H = 0$ during the expansion). Assuming ideal gas behaviour, we have

$$\frac{1}{2}mu^2 = -\int_{T_s}^{T_f} C_p \mathrm{d}T \tag{3.4}$$

where ½ mu^2 is the kinetic energy of the beam molecules and $C_p\mathrm{d}T = \mathrm{d}H$ is the change in enthalpy of the molecules within the source as they undergo supersonic expansion. T_s and T_f are the temperatures of the source and molecular beam, respectively. Since T_f is small relative to T_s, we have $T_s - T_f \approx T_s$. Also, assuming C_p is not temperature dependent, we can set $C_p = \gamma R/(\gamma\text{-}1)$, where $\gamma = C_p/C_V$. Evaluating (3.4) then gives

$$\frac{1}{2}mu^2 = \left(\frac{\gamma R}{\gamma\text{-}1}\right)T_s \tag{3.5}$$

Rearranging yields the beam terminal velocity.

$$u = \left(\frac{2RT_s}{m}\frac{\gamma}{(\gamma\text{-}1)}\right)^{1/2} \tag{3.6}$$

We see from Equation (3.6) that the terminal velocity of a supersonic molecular beam depends on the mass of the beam gas, with light gases achieving higher speeds than heavier gases. A beam of He has a terminal velocity of around 2400 ms^{-1}, while for HCl it is much lower, at around 500 ms^{-1}. Higher beam velocities for heavier molecules may be achieved by 'seeding' the heavier molecule in a light carrier gas so as to achieve a lighter 'average mass' for the beam molecules; a beam of 1% HCl in He, for example, has a terminal velocity of around 2100 ms^{-1}.

Supersonic beams by definition travel faster than the local speed of sound, which results in a complicated shock wave structure consisting primarily of a 'barrel shock' wave that surrounds the beam and a 'Mach disk' that intersects the beam axis. Immediately in front of the nozzle orifice is a 'zone of silence', which is not disturbed by shock waves. By placing a skimmer in the zone of silence, 1-2 cm from the nozzle, it is possible to create a collimated beam which is not disturbed by turbulence from the shock waves. The skimmer is shaped so as to pass molecules from the core of the beam, while deflecting the barrel shock wave and preventing the Mach disk from forming.

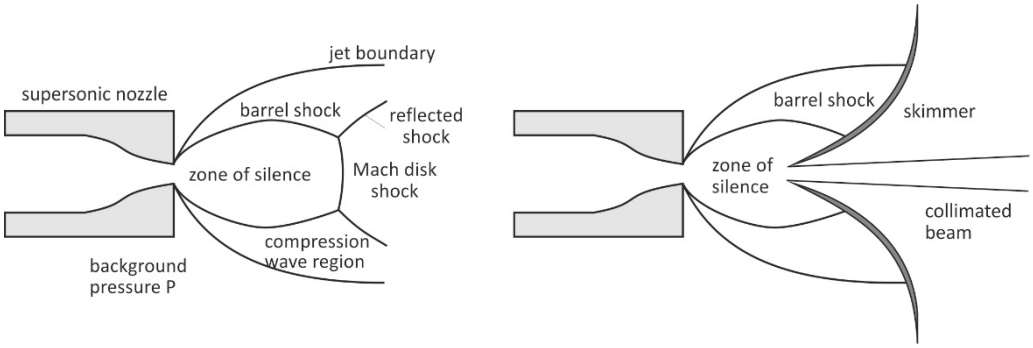

3.3.2 Controlling the beam velocity

In the previous section we learnt that the velocity of a molecular beam could be controlled by seeding the molecule of interest in a suitable buffer gas. Depending on the seed ratio, beam velocities can be achieved that range between the terminal velocity of the buffer gas and the terminal velocity of the seed gas (see Equation 3.6). A range of other techniques have been developed that allow control of the beam velocity, many of which allow access to a range of beam velocities outside that determined simply by the thermodynamics of the supersonic expansion.

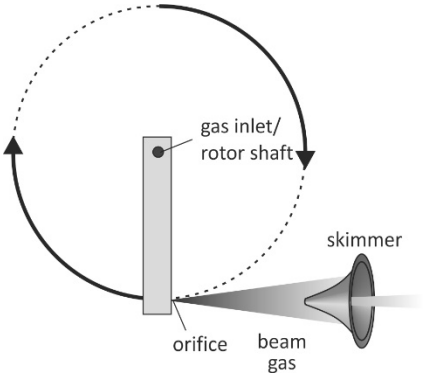

After seeding, the simplest method for speeding up or slowing down a molecular beam is to mount the source on the end of a rotating assembly, as shown on the left. The lab-frame velocity of the resulting beam is then the sum of the beam velocity resulting from the expansion and the velocity of the source. While this is a completely general technique, it is technically quite difficult to implement.

Recently, there has been a great deal of interest in using molecular beams to create ultracold molecules in order to study quantum mechanical effects that occur when chemical reactions are carried out at extremely low temperatures. The molecules in a molecular beam are already very cold. The velocity distribution within a supersonic molecular beam typically corresponds to a temperature of the order of a few Kelvin; however, the entire distribution is moving at the velocity of the molecular beam. The problem therefore becomes one of slowing the beam velocity distribution down. Various methods have been developed in which electric or magnetic fields are used to select a slow subset of beam molecules, and/or to slow the selected molecules down to much lower velocities. We will look at one example, the 'Stark decelerator', which uses the Stark effect to slow down the beam molecules.

When a molecule with a permanent dipole is subjected to an external field, its energy is lowered by the Stark effect if its dipole is aligned parallel to the field (a lower Stark state), and raised if its dipole is aligned antiparallel to the field (an upper Stark state). In an inhomogeneous electric field, lower Stark states can lower their energy by moving to regions of higher field - and for this reason are sometimes known as `high-field-seeking states' – while upper Stark states can lower their energy by moving to regions of lower field, and are also known as `low-field-seeking states'.

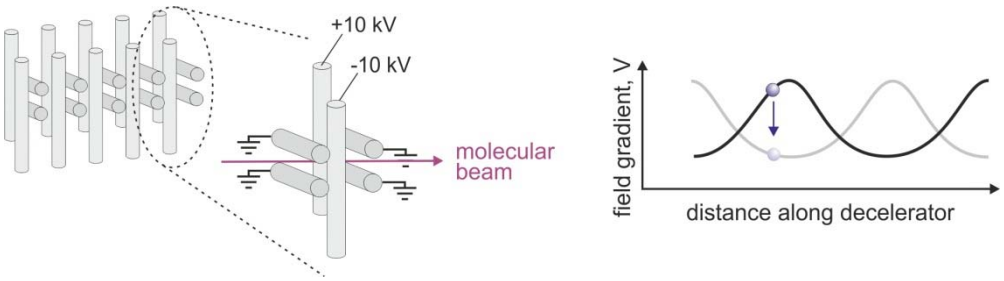

The Stark decelerator uses time-varying electric fields to decelerate a 'velocity slice' from a molecular beam to zero velocity. The decelerator is shown schematically above. It consists of alternate pairs of electrodes, with every second pair biased at high voltage and the remaining pairs grounded. When travelling between a grounded electrode and one at high potential, a molecule in a low-field-seeking Stark state will be climbing a potential gradient and will be slowed down. If the potential applied to the rods were static, once the molecule had passed the high-field electrode it would then accelerate down the potential gradient on the other side of the electrode and convert the potential energy it had gained back into kinetic energy. However, if as the molecule nears the high-potential electrode, the electrode potentials are switched (so that those at high potential are now grounded, and vice versa), the molecule again finds itself climbing a potential gradient, and is slowed further, and so on. Tens or even hundreds of deceleration stages can be used, depending on the desired final velocity. Note that only a certain fraction of beam molecules are decelerated, whose initial velocity, position, and quantum state place them in phase with the switching frequency of the decelerator.

3.3.3 Polarised laser photolysis

Radical species for reaction dynamics experiments are often generated through laser photolysis of a suitable precursor molecule. If a polarised laser is used to carry out the photodissociation, the radical is often formed with a highly anisotropic velocity distribution, providing a reference direction for measurements of product velocity distributions.

The transition dipole vector $\boldsymbol{\mu}_{if}$ for the excitation from state *i* to state *f* that leads to dissociation is given by

$$\boldsymbol{\mu}_{if} = \langle \psi_f | \hat{d} | \psi_i \rangle \qquad (3.7)$$

where $\hat{d}$ is the electric dipole operator. Radical precursors tend to be either diatomic or linear triatomic molecules, and in these molecules the transition dipole vector will generally lie either parallel or perpendicular to the bond. For an electric dipole transition to occur, the transition dipole must interact with the electric vector $\boldsymbol{\varepsilon}$ of the laser pulse. The transition probability P_{if} is then

$$P_{if} = |\boldsymbol{\mu}_{if}.\boldsymbol{\varepsilon}|^2 = \mu_{if}^2 \varepsilon^2 \cos^2\theta \qquad (3.8)$$

where θ is the angle between $\boldsymbol{\mu}_{if}$ and $\boldsymbol{\varepsilon}$. The probability of a molecule absorbing a photon and dissociating is therefore strongly dependent on the angle between the transition dipole and the electric field vector of the light. When linearly polarised light is incident on a randomly oriented sample of gas, immediately following excitation the transition dipoles of the excited state molecules will have a $\cos^2\theta$ angular distribution about the laser polarisation vector. If the transition dipole lies parallel to the breaking bond, this will translate into a $\cos^2\theta$ distribution of the fragment velocities about the laser polarisation vector, while if the transition

dipole lies perpendicular to the breaking bond then a $\sin^2\theta$ distribution will result. This is illustrated below for Cl atoms formed in the polarised laser dissociation of Cl_2 via a perpendicular transition. The $\sin^2\theta$ distribution is clearly visible, with signal intensity peaking at right angles to the laser polarisation vector (marked in white on the images).

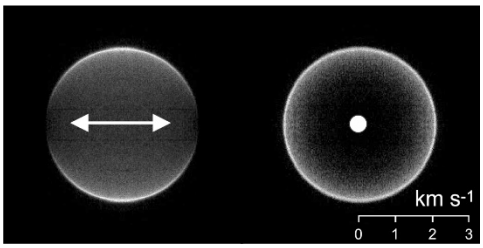

3.5 Cross section measurements

Total cross sections can be measured by measuring the attenuation of a molecular beam as it passes through a collision chamber containing the scattering gas of interest, as shown in the figure below.

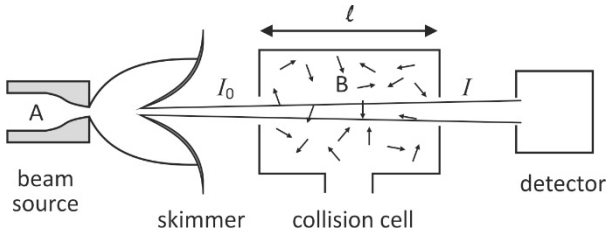

If the path length through the scattering chamber is ℓ and the number density of the scattering gas is n, we can determine the mean free path λ and the collision cross section from the Beer-Lambert law.

$$I = I_0 \exp(-n\sigma\ell) = I_0 \exp\left(-\frac{\ell}{\lambda}\right) \qquad \text{with} \qquad \lambda = \frac{1}{n\sigma} \tag{3.9}$$

The beam intensity transmitted through the collision cell in the presence (I) and absence (I_0) of the scattering gas are measured, the path length ℓ is known, and the number density n is calculated from the measured pressure and temperature of the collision cell, assuming the ideal gas law.

Note that the measured attenuation cross section is the sum of the cross sections for all processes that scatter the incident beam. For an atomic beam and scattering gas, this is simply the elastic scattering cross section σ_E, while for an atomic or molecular beam with a molecular scattering gas, the cross section is the sum of the elastic and inelastic (including reactive) cross sections i.e. $\sigma = \sigma_E + \sigma_{IN}$.

3.6 Control of initial quantum states

There are numerous ways in which the initial quantum states of the reactant molecules can be selected. Simply expanding the molecules in a molecular beam usually yields molecules in their ground vibrational state and low rotational states, while electronically or vibrationally excited states may be prepared by laser excitation from the ground state immediately prior to the collision process of interest.

Dipolar molecules, such as heteronuclear diatomics or symmetric tops, may be prepared in single rotational states by exploiting their trajectories through an inhomogeneous electric field. In Section 3.3.2 we met the Stark effect, and noted that in an inhomogenous electric field, molecules in lower Stark states (dipole aligned parallel to the field) are 'high-field seeking', while those in upper Stark states (dipole aligned antiparallel to the field) are 'low-field seeking'.

State selection of diatomics is limited to a few molecules with very large dipole moments, and we will focus here on state selection of symmetric top molecules using a hexapole field. A hexapole state-selector consists of six metal rods mounted on an inscribed radius r_0, with positive and negative high voltages applied to alternate rods, as shown below.

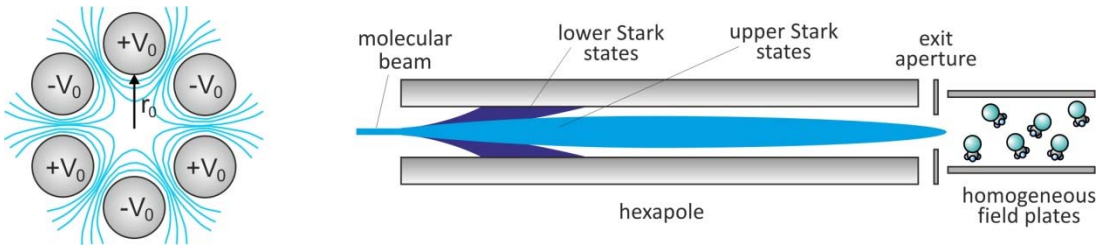

The rotational state of a symmetric top molecule is defined by three quantum numbers: the total angular momentum, J, the projection K of $\boldsymbol{J}$ onto the molecular axis; and the projection M_J of $\boldsymbol{J}$ onto a lab-frame axis, in this case the external field direction. The rotational motion is precessional: the molecular axis precesses about the total angular momentum vector $\boldsymbol{J}$, which in turn precesses about the lab-frame axis. Solving the equations of motion for a symmetric top molecule through a hexapole field yields simple harmonic oscillator solutions for the radial coordinate. Molecules in lower Stark states follow exponential trajectories that diverge from the hexapole axis, and are lost from the molecular beam. Conversely, upper Stark states follow sinusoidal trajectories, $r(t) \propto \sin\omega t$, which focus back to the axis at a distance that depends on the rotational state $|JKM_J\rangle$ and the potential V_0 applied to the hexapole rods, as determined by the oscillation frequency, ω.

$$\omega = \left(\frac{6V_0 d}{m r_0^3} \frac{|KM_J|}{J(J+1)} \right)^{1/2} \qquad (3.10)$$

where m and d are the mass and dipole moment of the molecule, and r_0 is the inscribed radius of the hexapole rods. The dependence of ω on both V_0 and the rotational state of the molecule means that the hexapole potential can be chosen to focus any desired rotational state with $KM_J \neq 0$ onto the beam axis at the hexapole exit. Other non-focusing rotational states may be eliminated from the beam by using an iris or pinhole to allow only the focused state of interest to exit the hexapole.

As well as being used for rotational state selection, the hexapole technique can also be used to create a beam of spatially oriented symmetric top molecules. The upper Stark states transmitted through the hexapole are all aligned with their dipoles opposing the local applied electric field, but are not yet uniformly oriented in space, since the hexapole field is inhomogeneous. In order to spatially orient the beam it is allowed to pass adiabatically (i.e. without changing quantum state) into a region of weak homogeneous electric field maintained between a pair of parallel plates positioned directly after the hexapole. As the beam leaves the hexapole the molecular dipoles rotate in space to line up against the new homogeneous field and orientation is achieved. A homogeneous field of only around 2 V cm^{-1} or more is required in order to ensure that the upper Stark states remain well-defined and thereby to achieve some degree of molecular

orientation. However, considerably stronger fields are often required in order to overcome coupling of ***J*** to any non-zero nuclear spins within the molecule in order to achieve optimum orientation.

The degree of orientation is determined by the rotational states of the molecules in the beam. In the strong-field case, where coupling of ***J*** to the electric field is much stronger than coupling to any non-zero nuclear spins, the average angle between the electric field vector and the molecular dipole (i.e. the precession angle) for a given $|JKM_J\rangle$ state is given by

$$\langle\cos\theta\rangle = \frac{KM_J}{J(J+1)} \qquad (3.11)$$

In the second half of the course, you will look an example in which the hexapole orientation method was used to study steric effects in the Rb + CH_3I reaction.

Numerous other techniques are available for generating spatially oriented molecules for dynamics studies. If you would like to read more about these methods, a detailed discussion can be found in a recent review article[4].

3.7 Measurement of final velocities

3.7.1 Crossed beam experiment with rotating mass spectrometer

One of the most commonly used methods for measuring the product velocity (speed and angular) distribution is the crossed molecular beam technique. Two molecular beams containing the reactants of interest are crossed, usually at right angles, and reaction products scatter out from the crossing region. A rotatable detector, normally a quadrupole mass spectrometer, is then used to measure the product flux as a function of angle. At each angle, an arrival time distribution is recorded for the product of interest, which can be transformed into a speed distribution for products scattered in that direction, since the distance from the crossing region to the detector is known. By recording a speed distribution at each angle, the complete velocity distribution can be measured. Note that this type of detection is not product state-selective.

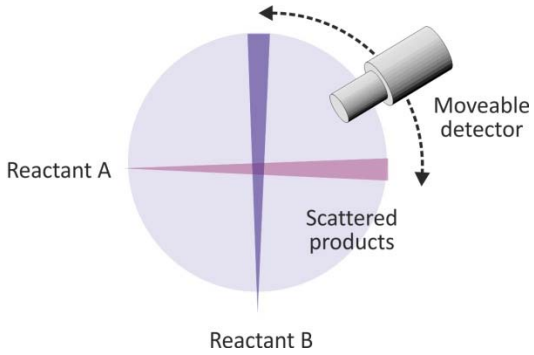

[4] C. Vallance, 'Generation, characterisation, and applications of atomic and molecular alignment and orientation', *Phys. Chem. Chem. Phys.*, 13 14427-14441 (2011).

Some crossed molecular beam instruments allow the crossing angle of the beams to be varied to provide control over the collision energy. Crossing the beams at a smaller angle reduces the collision energy, while moving to larger crossing angles (i.e. closer to a 'head on') geometry increases the collision energy.

We noted in Section 1.2 that the velocity of the centre of mass is conserved throughout a collision. We should also note that different experimental setups will yield different velocities for the centre of mass; for example, as we increase the beam crossing angle in a crossed molecular beam experiment, the velocity of the centre of mass becomes smaller. In order to compare the results of different experiments (measured in the so-called 'laboratory frame' or 'lab frame' of reference), we normally subtract the velocity of the centre of mass from our measured velocity distribution. The result is the velocity distribution that we would observe if we were travelling along with the centre of mass, and for this reason it is called the *centre-of-mass (CM) frame* velocity distribution. The 'lab to CM frame transformation', as the subtraction is called, will be covered in detail in Section 3.9. However, the transformation is shown in terms of a *Newton diagram* below.

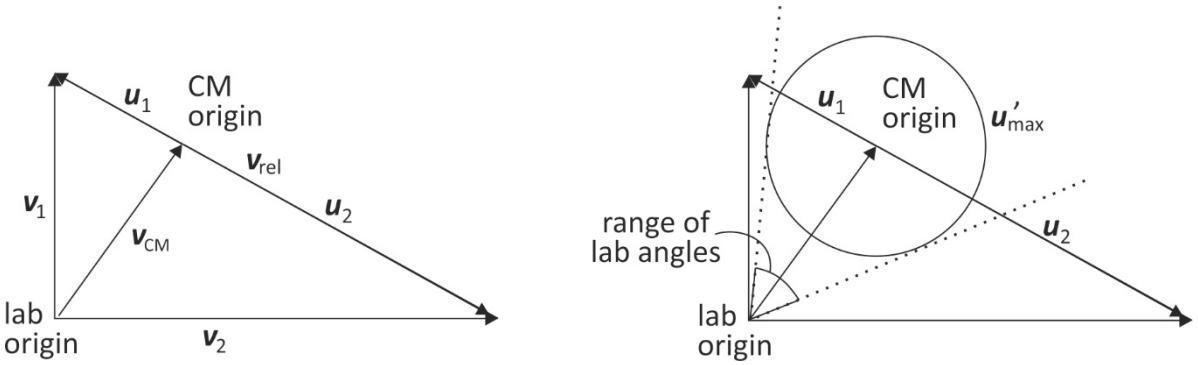

The Newton diagram on the left above shows both the lab-frame and CM-frame velocities of the reactants, together with the velocity of the centre of mass, v_{CM}. The lab-frame velocities are labelled v_1 and v_2, and the CM frame velocities are labelled u_1 and u_2. Note that in the CM frame, the reactants collide head on along the relative velocity vector. As noted in Section 1.9, the relative velocity vector is an axis of symmetry for the collision, and scattering is therefore symmetric about this direction. The reaction products will have some maximum velocity u_{max}', determined from energy conservation requirements (see Section 1.3), and will therefore scatter somewhere within the circle of radius u_{max}' centred on the CM-frame origin. We see that in the lab-frame, scattering is only possible over a rather restricted range of angles. The rotatable detector in a crossed beam experiment therefore does not need to sample the full 360 degrees about the crossing region.

The data from a crossed molecular beam experiment is normally shown in the form of a CM-frame *flux-velocity-angle contour map*, in which the radial coordinate corresponds to product speed, the angular coordinate corresponds to scattering angle, and the intensity at a given point on the map corresponds to the flux of products scattered in the corresponding direction. Some examples of flux-velocity-angle contour maps are shown below, illustrating reactions with various different scattering behaviours. The plots can be analysed to extract differential cross sections, product speed and internal state distributions, all of which provide detailed information on the reaction mechanism. The dynamics leading to these different scattering behaviours will be examined in the second half of the course.

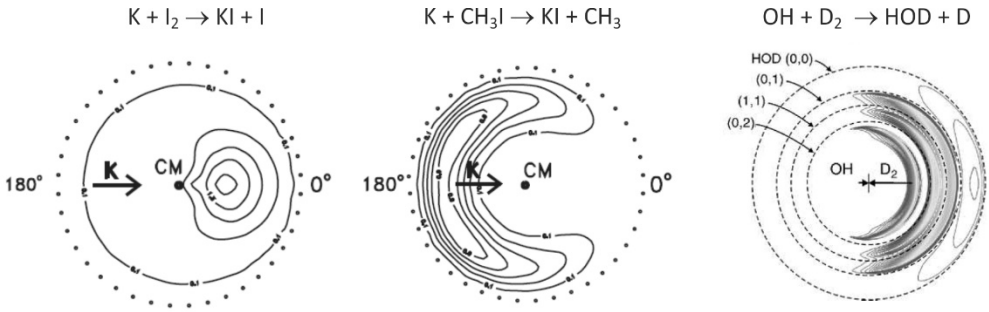

3.7.3 Velocity-map imaging

The crossed molecular beam experiments described above build up the product velocity distribution angle by angle. This is a time consuming and labour-intensive process. More recently, laser-based techniques have been developed which allow the complete product scattering distribution to be recorded in essentially a single measurement, with the added capability of product quantum state selection. Velocity-map imaging can be combined either with a single molecular beam (for example, in photodissociation studies), or with crossed beam experiments. Typical velocity-map imaging setups for both types of study are shown below.

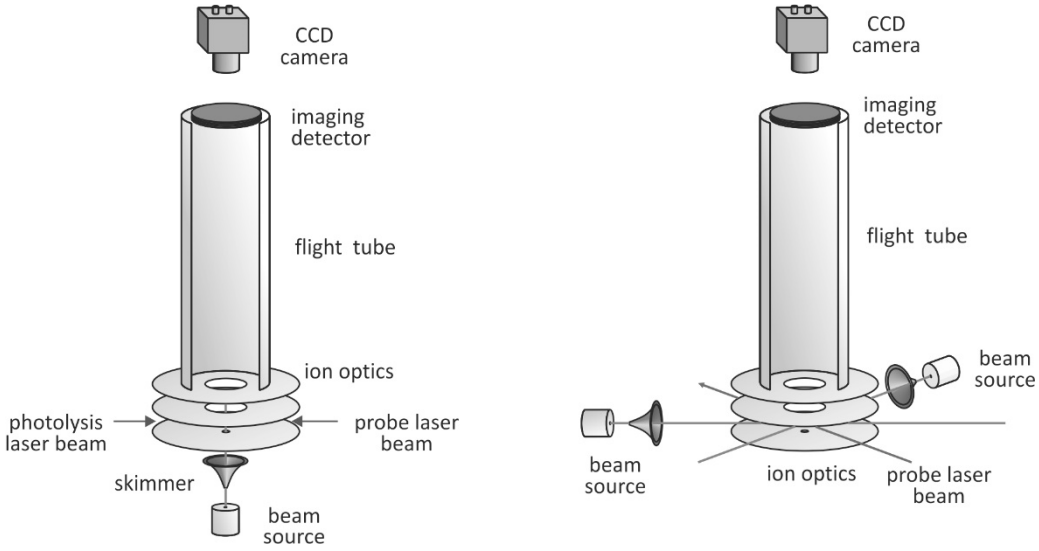

The essential elements of the setup are a set of electrostatic lenses, a flight tube, and a position sensitive detector. The chemical process under study will generally yield products flying out from the interaction region (e.g. the point where two molecular beams cross in the case of a crossed beam experiment, or where a laser and molecular beam cross in the case of a photodissociation experiment) in a 'Newton sphere' in all directions. To perform a velocity mapping measurement, the reaction product of interest is ionized (state-selectively if desired) within the electrostatic lens system by a laser pulse. The ionization step usually employs a 'REMPI' process of the type described in Section 3.8.3. As soon as the neutral products are ionized, they 'feel' the electric field maintained within the electrostatic lens system. The field plays three simultaneous roles. It accelerates the ions along the flight tube to the detector, it maps all ions with the same velocity component in the detector plane onto the same point on the detector, and it compresses the Newton sphere for a given ion mass into a 'pancake' as it strikes the detector. The field accelerates all ions to the same kinetic energy, and since $K = \frac{1}{2}mv^2$, this means that ions of different masses

fly to the detector at different velocities, as shown below, and are therefore separated in time when they reach the detector. This is the principle underlying *time-of-flight mass spectrometry*. In velocity-map imaging experiments, the ion of interest can easily be *mass-selected* by time-gating the detector (turning the detector on briefly at the appropriate time) so that only ions of the desired mass are imaged.

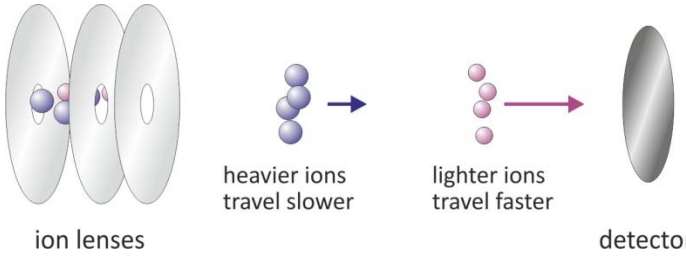

The detector consists of a pair of microchannel plates (MCPs) coupled to a phosphor screen. The MCPs convert each incident ion into a pulse of electrons, and the phosphor converts the electrons into a flash of light which can be imaged on a CCD camera placed behind the screen. The resulting image is a two dimensional projection of the complete three-dimensional (CM-frame) velocity distribution of the nascent reaction products. Some example images recorded for a range of chemical systems are shown below.

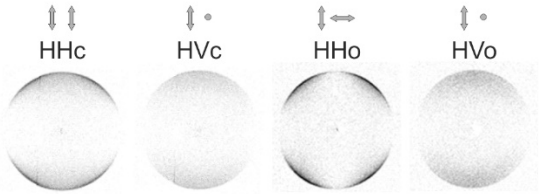

$O(^1D)$ atoms from photofragmentation of O_2, recorded for different pump and probe laser polarisations (Dave Parker, Nijmegen, and Claire Vallance, Oxford).

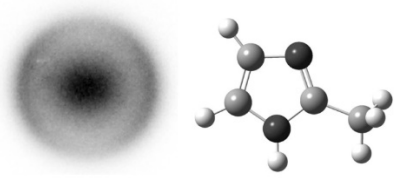

H atoms from the photofragmentation of 2-methylimidazole (Vas Stavros, Warwick)

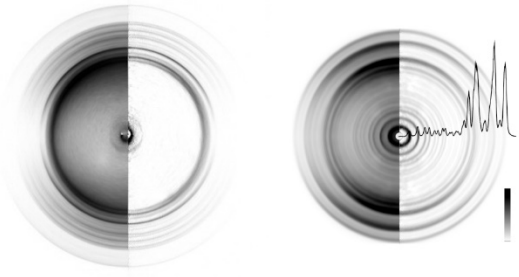

Proton and electron images following excitation of the V state in HCl (Hans-Peter Loock, Queens University, Canada)

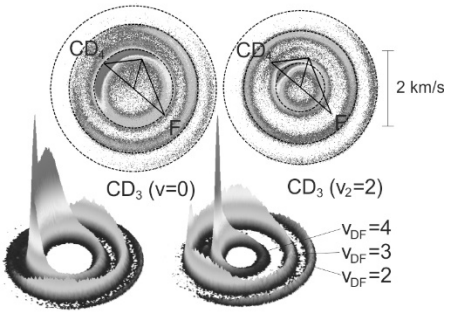

CD_3 products from a crossed beam study on the $F + CD_4 \rightarrow HF + CD_3$ reaction (Kopin Liu, Taipei)

In many cases, the scattering distribution has an axis of cylindrical symmetry, and the full 3D scattering distribution can be recovered from the 2D projection using a mathematical transform called the inverse Abel transform. In the example below, the image on the left is a typical 2D 'crushed' image. The Abel

inversion 'reinflates' the image and extracts the centre slice (centre image). Rotating the slice about the axis of cylindrical symmetry returns the 3D distribution (right image).

A technique called 'slice' imaging relies on carefully time-gating the detector in order to allow the central slice of the 3D distribution to be recorded directly, eliminating the need for the Abel inversion.

3.7.3 Doppler profiles and pump-probe experiments

As we shall see in Section 3.8, various types of absorption spectroscopy may be used to detect product molecules state selectively. The spectral linewidths of the rovibronic transitions excited in such measurements are determined by the product velocity distribution through Doppler broadening of the peaks. A moving molecule has a Doppler shift given by

$$\nu = \left(1 - \frac{v_z}{c}\right)\nu_0 \qquad (3.12)$$

where ν_0 is the absorption frequency of the molecule at rest, ν is the absorption frequency of the molecule moving with a velocity component v_z along the laser propagation direction, and c is the speed of light.

If the frequency bandwidth of the probe laser is much narrower than the width of the spectral line, then the spectral lineshape constitutes a one-dimensional projection of the product velocity distribution onto the laser propagation axis. If several one-dimensional projections are recorded, enough information is obtained to reconstruct the entire three-dimensional velocity distribution.

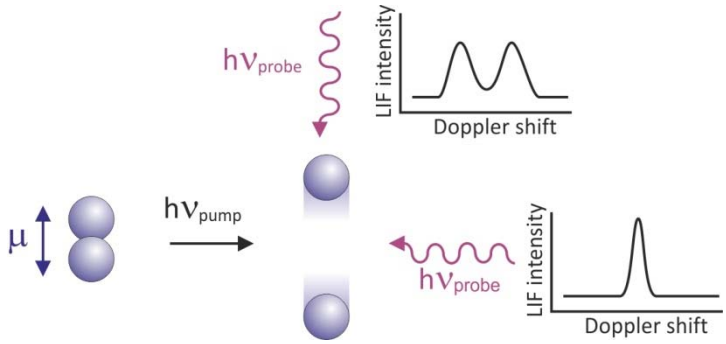

Doppler profile measurements are usually carried out as the detection, or 'probe', step in a laser pump-probe experiment. We first met laser pump-probe experiments in Section 3.2 as an example of a technique for achieving temporal isolation of collisions. A simple example, shown above, is the dissociation of a diatomic molecule via a parallel transition (i.e. the transition dipole lies along the bond). When the pump laser is polarised along the transition dipole/bond axis μ, the molecule dissociates, and the atomic products fly in the up and down directions, as shown. On the right of the figure we see the two very different Doppler lineshapes recorded by a probe pulse travelling either parallel or perpendicular to the recoil

direction of the fragments. When the probe laser beam propagates along the recoil direction of the photofragments, the line profile is split into two peaks, corresponding to fragments flying towards or away from the laser beam. Doppler profiles can be recorded for individual product quantum states, simply by tuning the probe laser wavelength to a transition involving the state of interest. This allows complete product velocity distributions to be recorded as a function of product quantum state.

The pump-probe/Doppler profile technique can also be used to study photoinitiated bimolecular reactions. The technique requires that one of the reactants can be prepared by laser photolysis of a suitable precursor molecule (for example, oxygen atoms can be prepared by dissociation of O_2, N_2O, and various other precursors; chlorine atoms can be prepared by photolysis of Cl_2, and so on). A gas mixture is prepared, either in a beam or a bulb, that contains the precursor molecule (AX) and the second reactant (B), and the pump-probe sequence is as follows:

$AX + h\nu \rightarrow A + X$	Pump (photoinitiation)
$A + B \rightarrow P$	Bimolecular reaction
$P + h\nu' \rightarrow P^*$	Probe (LIF or REMPI)

In the pump step, the precursor molecule is dissociated to form the reactant A. The two reactants then react to form products P, and in the probe step either LIF or REMPI is used to record appropriate Doppler profiles for the product quantum states of interest. The details of extracting product velocity distributions from the measured Doppler profiles are somewhat complicated, but the basic principle is easy to understand, and is shown in the Figure below. Photolysis of the precursor forms reactant A expanding in a Newton sphere with a well-defined velocity distribution (shown on the left below). Following reaction, forward scattered products lie on a larger Newton sphere than that for the reactant A (below centre), while backward scattered products lie on a smaller sphere (below right). This will lead to very different Doppler profiles for the two cases. Assuming the Newton sphere of A has been well characterised in separate experiments, the data can be analysed to extract the velocity distribution (and therefore the speed and angular distribution/differential cross section) of the reaction products.

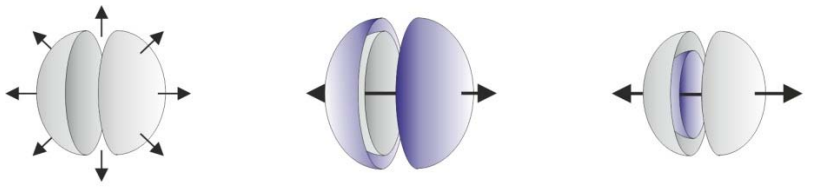

3.8 Measurement of final quantum states

3.8.1 Infrared chemiluminescence

Chemical reactants often produce products with significant amounts of internal excitation. Chemiluminescence employs a spectroscopic analysis of light emitted by these excited states to measure the relative populations of the states.

A chemiluminescence experiment is typically carried out in a fast flow system under steady state conditions, using an experimental setup similar to that shown in the diagram below. To avoid collisional relaxation of the newly formed reaction products, the collision chamber is maintained at a low background pressure of $\sim 10^{-5}$ mbar or less. A water-cooled or liquid-nitrogen-cooled jacket stops any particles that strike the wall, further helping to prevent secondary collisions. During an experiment, two uncollimated jets (or better, supersonic beams) of reactants intersect, and are pumped away as fast as possible. Radiation emitted from the reaction zone is collected and focussed into an infrared spectrometer. From intensity measurements of the emission lines corresponding to assigned transitions between known (v,J) states, relative populations of the states can be inferred. The technique employs temporal isolation to observe the nascent reaction products, working on the principle that the time between collisions is greater than the radiative lifetime for infrared emission. As an example, in a study of the reaction Cl + HI $\rightarrow$ HCl + I, the time between collisions in the crossing region ($p \sim 10^{-1}$ to 10^{-2} mbar) was around 10^{-6} s, compared with an infrared emission lifetime for HCl of of $\sim 10^{-9}$ s.

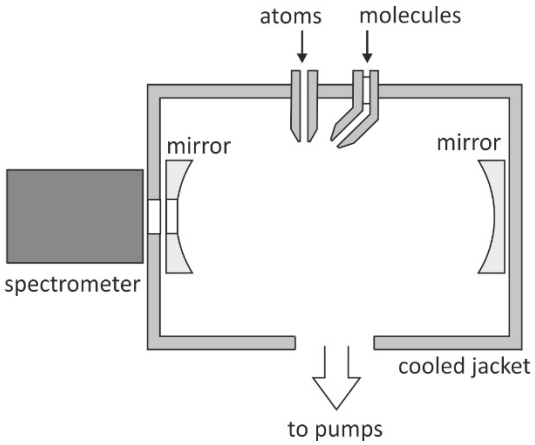

Note that since the technique is a type of emission spectroscopy, it does not give any information about population of the ground state. Chemiluminescence data can be used to determine the relative rates of reaction to produce different product quantum states, but since absolute product yields are not recorded, it cannot give absolute rates.

3.8.2 Laser-induced fluorescence (LIF)

In the previous section, we saw how emission spectroscopy could be used to determine the internal state distributions of newly formed reaction products. An alternative approach is to use absorption spectroscopy, which has the added advantage of being sensitive to the population of the ground state. However, since a typical pump-probe experiment may produce only a few hundred product molecules per laser cycle, and these will be present amongst much higher concentrations of other species, such as unused reactants and background gases, a typical 'Beer-Lambert' type absorption measurement is completely inadequate. We require a technique that is both extremely sensitive and highly specific to the chemical species of interest. Laser-induced fluorescence (LIF) is one technique that matches these requirements. The technique requires that the molecule under study has a fluorescent excited state that is accessible from the electronic ground state, and that the spectroscopy of the electronic transition is well understood. The technique is illustrated schematically below on the left.

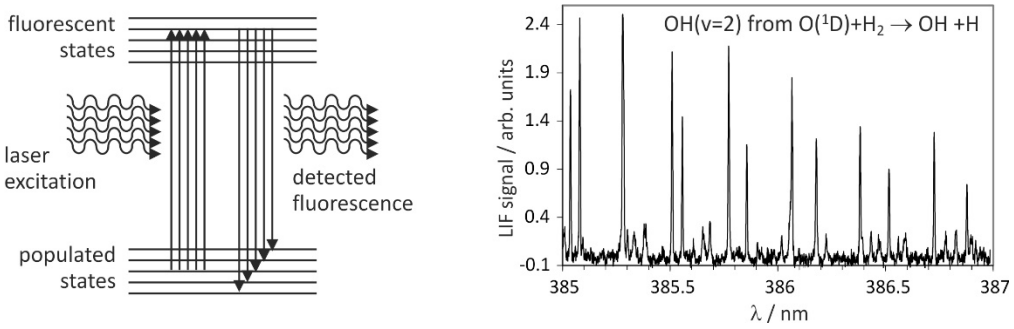

Nascent products are excited to the upper state, and the photons emitted as the excited state relaxes are detected, with the measured signal being proportional to the original population of the lower state. By scanning the excitation laser over the various accessible rovibronic transitions from the ground state, the rovibrational state populations of the nascent products may be determined. In order to compare the signals from two states, the LIF signals must be corrected to take account of the differing absorption cross sections of the lower state and emission cross sections of the upper state(s) involved in the transitions. LIF is widely used for detection of small molecules such as OH and NO produced in a pump-probe reaction scheme. On the right in the figure above is shown a LIF spectrum for OH molecules formed in the insertion reaction $O(^1D) + H_2 \rightarrow OH + H$.

3.8.3 Resonance-enhanced multiphoton ionization (REMPI)

A second technique that satisfies the sensitivity and selectivity requirements outlined above is resonance-enhanced multiphoton ionization (REMPI). Selective ionization of the product molecule of interest makes detection relatively straightforward. Ions can be steered towards a detector by means of an appropriately electric field, and particle multiplier detectors capable of detecting single ions have been widely available for several decades. Single photon ionization of most molecules is unfeasible, since their ionization energies correspond to photons in the soft X-ray region, which are not easy to generate in most laboratories. Instead, ionization is usually brought about through essentially simultaneous absorption of two or more photons, as shown in the figure below.

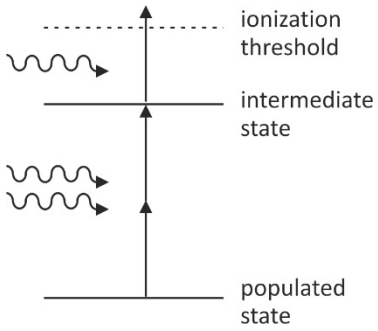

The first photon accesses a 'virtual state'. Such a state is not a solution of the molecular Hamiltonian, but a very short lived state of the 'molecule + photon' system. As long as a second photon arrives sufficiently quickly, requiring high light intensities such as those found in a laser pulse, the virtual state can absorb a photon to reach a real or virtual state of higher energy. Non-resonant multiphoton ionization, in which none of the intermediate levels accessed by successive photon absorptions correspond to real levels of the molecule, is not a particularly efficient process. However, when one of the intermediate states does

correspond to an actual state of the molecule, the ionization efficiency is increased enormously, often by orders of magnitude, and we have resonance-enhanced multiphoton ionization. REMPI schemes are usually labelled in terms of the number of photons required to reach the resonant state and the number of photons required to ionize from the resonant state. So, for example, in a (2+1)REMPI process, two photons are absorbed to take the molecule from the ground state to the intermediate state, and a third photon ionizes the molecule from this state.

Efficient REMPI schemes are available for a wide range of molecules, and for this reason the technique is more widely used than LIF detection. The photon energy used for the initial transition to the resonant state can be tuned to ionize a specific quantum state of the molecule of interest, and scanning the laser wavelength to record a REMPI absorption spectrum allows product quantum state distributions to be determined.

The resonant state employed in a REMPI scheme is often a Rydberg state (i.e. a very high-lying state) of the molecule. Such states have low ionization potentials, and can be *field ionised* simply by exposing the molecule to a sufficiently strong electric field. In an alternative detection technique to REMPI, known as *Rydberg tagging*, a laser is used to excite molecules to a Rydberg state without ionising them. The neutral 'Rydberg tagged' molecules are then allowed to fly to the detector, where they are ionized by an electric field immediately prior to detection. Rydberg tagging is a very useful detection technique for experiments in which creating ions or using electric fields to extract ions in the interaction region would disturb the collisional process under study. However, it is also used in other situations. Some examples will be given in the second half of this lecture course.

Both LIF and REMPI can be combined with Doppler resolved measurements (Section 3.7.3) in order to obtain information on the product velocities. REMPI is also commonly combined with time-of-flight mass spectrometry or velocity-map imaging to obtain velocity information. A time-of-flight profile provides a one-dimensional projection of the velocity distribution, while velocity-map imaging yeilds a two-dimensional projection.

3.9 Comparison of results: the lab-to-centre-of-mass frame transformation

As noted in Section 3.7, the product scattering distributions recorded in a reaction dynamics experiment are recorded in some fairly arbitrary *laboratory* (lab) *frame* of reference, determined by the geometry of the experiment. To compare the results of different experiments (and also to compare experiment with theory) we need to transform the results into a common frame of reference called the *centre of mass frame*. In the CM frame, the observer is travelling along with the centre of mass of the system, so the total momentum in this frame is zero, and the reactants appear to undergo a head on collision at the position of their centre of mass, as illustrated below.

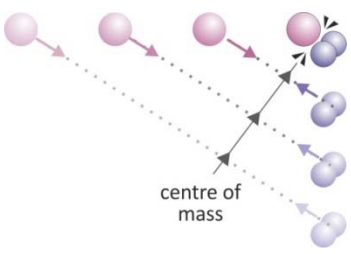

The CM frame is independent of experimental geometry, allowing results from different types of experiments to be compared, and also provides a much more intuitive picture of the collision dynamics than any lab frame. As an example, 'forward' and 'backward' scattering is always defined relative to the CM frame, whereas in the lab frame these terms can be ambiguous to say the least.

Analogy: In some sense, choosing to transform all data from reaction dynamics experiments into the CM frame is a little like transforming all data from NMR spectroscopy experiments into units of chemical shift. The transformation allows data from different dynamics experiments (c.f. different spectrometers in NMR) to be compared directly.

3.9.1. Calculations involving the CM and lab frames

We will now work through a lab to CM frame transformation for an elastic collision. It is straightforward to extend the following to inelastic or reactive collisions; all you have to do is add or subtract the appropriate energy change ($\Delta_r H$ in the case of a reaction) from the energy of the collision products. While working through the following analysis, note that velocity is a vector quantity.

Usually, we know the velocities of the two particles before the collision, $\boldsymbol{v}_1$ and $\boldsymbol{v}_2$. These are our 'lab frame' velocities. The kinetic energies of the two particles are $K_1 = ½\, m_1\boldsymbol{v}_1^2$ and $K_2 = ½\, m_2\boldsymbol{v}_2^2$, and the total kinetic energy is

$$K = K_1 + K_2 = ½\, m_1\boldsymbol{v}_1^2 + ½\, m_2\boldsymbol{v}_2^2 \qquad \text{(lab frame)} \qquad (3.13)$$

At some point we will need to determine the velocities in the CM frame – call them $\boldsymbol{u}_1$ and $\boldsymbol{u}_2$ to differentiate them from the lab frame velocities. This is a simple calculation to do. Remember that the centre of mass frame is just the frame in which we are travelling along with the centre of mass. This means that all we have to do to go from lab frame to CM frame velocities is subtract the velocity $\boldsymbol{v}_{CM}$ of the centre of mass.

$$\boldsymbol{u}_1 = \boldsymbol{v}_1 - \boldsymbol{v}_{CM}$$

$$\boldsymbol{u}_2 = \boldsymbol{v}_2 - \boldsymbol{v}_{CM} \qquad (3.14)$$

We can determine $\boldsymbol{v}_{CM}$ by noting that the total momentum of the system may be written either as the momentum of the centre of mass, $M\boldsymbol{v}_{CM}$, with M the total mass of the two particles, or as the sum of the momenta of the two individual particles.

$$M\boldsymbol{v}_{CM} = m_1\boldsymbol{v}_1 + m_2\boldsymbol{v}_2 \quad \Rightarrow \quad \boldsymbol{v}_{CM} = \frac{m_1\boldsymbol{v}_1 + m_2\boldsymbol{v}_2}{M} \qquad (3.15)$$

The fact that the total momentum is zero in the CM frame gives us another approach to finding the CM-frame velocities. Since $\boldsymbol{v}_{rel} = \mathbf{v}_1 - \mathbf{v}_2 = \mathbf{u}_1 - \mathbf{u}_2$, and $m_1\boldsymbol{u}_1 = -m_2\boldsymbol{u}_2$, we obtain

$$u_1 = \frac{m_2}{M}\boldsymbol{v}_{rel} \qquad \text{and} \qquad u_2 = \frac{m_1}{M}\boldsymbol{v}_{rel} \qquad (3.16)$$

In addition to defining the momentum associated with the motion of the centre of mass, we can also define the kinetic energy associated with this motion.

$$K_{CM} = \tfrac{1}{2} M \boldsymbol{v}_{CM}^2 \qquad (3.17)$$

Note that because the total momentum of the system has to be conserved, the velocity, momentum, and kinetic energy of the centre of mass are conserved throughout the collision (this is true for any type of collision, including inelastic and reactive ones). As noted earlier, energy 'tied up' in the motion of the centre of mass is therefore not available for the collision. For a reactive collision, this energy does not help overcome any activation barrier that might be present.

Having defined the total kinetic energy and the kinetic energy associated with the centre of mass, the remaining kinetic energy is of course the energy associated with relative motion of the two particles. This energy *is* available for the collision, and from Section 1.2 we recognise it as the collision energy, also sometimes referred to as the 'CM frame kinetic energy'.

$$K_{rel} = \tfrac{1}{2} \mu \boldsymbol{v}_{rel}^2 \qquad (3.18)$$

We have now determined all of the relevant parameters involving the reactants. The product velocites may be determined by requiring that momentum and kinetic energy (or total energy in the case of an inelastic or reactive collision) are conserved during the collision. Usually it is most straightforward to do this calculation in the CM frame, though it should work just as well in the lab frame, albeit with somewhat trickier algebra.

$$m_1\boldsymbol{u}_1 + m_2\boldsymbol{u}_2 = m_1\boldsymbol{u}_1' + m_2\boldsymbol{u}_2' \qquad \text{(momentum conservation)}$$

$$\tfrac{1}{2} m_1\boldsymbol{u}_1^2 + \tfrac{1}{2} m_2\boldsymbol{u}_2^2 = \tfrac{1}{2} m_1\boldsymbol{u}_1'^2 + \tfrac{1}{2} m_2\boldsymbol{u}_2'^2 \quad \text{(energy conservation)} \qquad (3.19)$$

These two equations simply constitute two equations in the two unknowns $\boldsymbol{u}_1'$ and $\boldsymbol{u}_2'$ (the final CM frame velocities). For an inelastic or reactive collision, the second equation would include an additional term containing the change in internal energy for an inelastic collision, or reaction enthalpy for a reactive collision. Recall that in the CM frame the total momentum is zero both before and after the collision. This simplifies the situation considerably, since the first equation becomes simply

$$m_1\boldsymbol{u}_1' + m_2\boldsymbol{u}_2' = 0 \qquad (3.20)$$

Once we have solved the equations to determine the CM frame velocities after the collision, we can find the equivalent lab frame velocities for comparison with experiment simply by adding on the velocity of the CM (which, remember, stays constant throughout the collision).

$$\boldsymbol{v}_1' = \boldsymbol{u}_1' + \boldsymbol{v}_{CM}$$

$$\boldsymbol{v}_2' = \boldsymbol{u}_2' + \boldsymbol{v}_{CM} \qquad (3.21)$$

SUMMARY

At this point, you should be well equipped with many of the basic concepts of molecular reaction dynamics. In the next four lectures these ideas will be developed in more detail and you will be introduced to a number of examples to illustrate the dynamics of a broad range of different chemical systems.